Volcanoes, the QBO, and Climate

Prof. Matthew Hitchman

Department of Atmospheric and Oceanic Sciences
University of Wisconsin - Madison

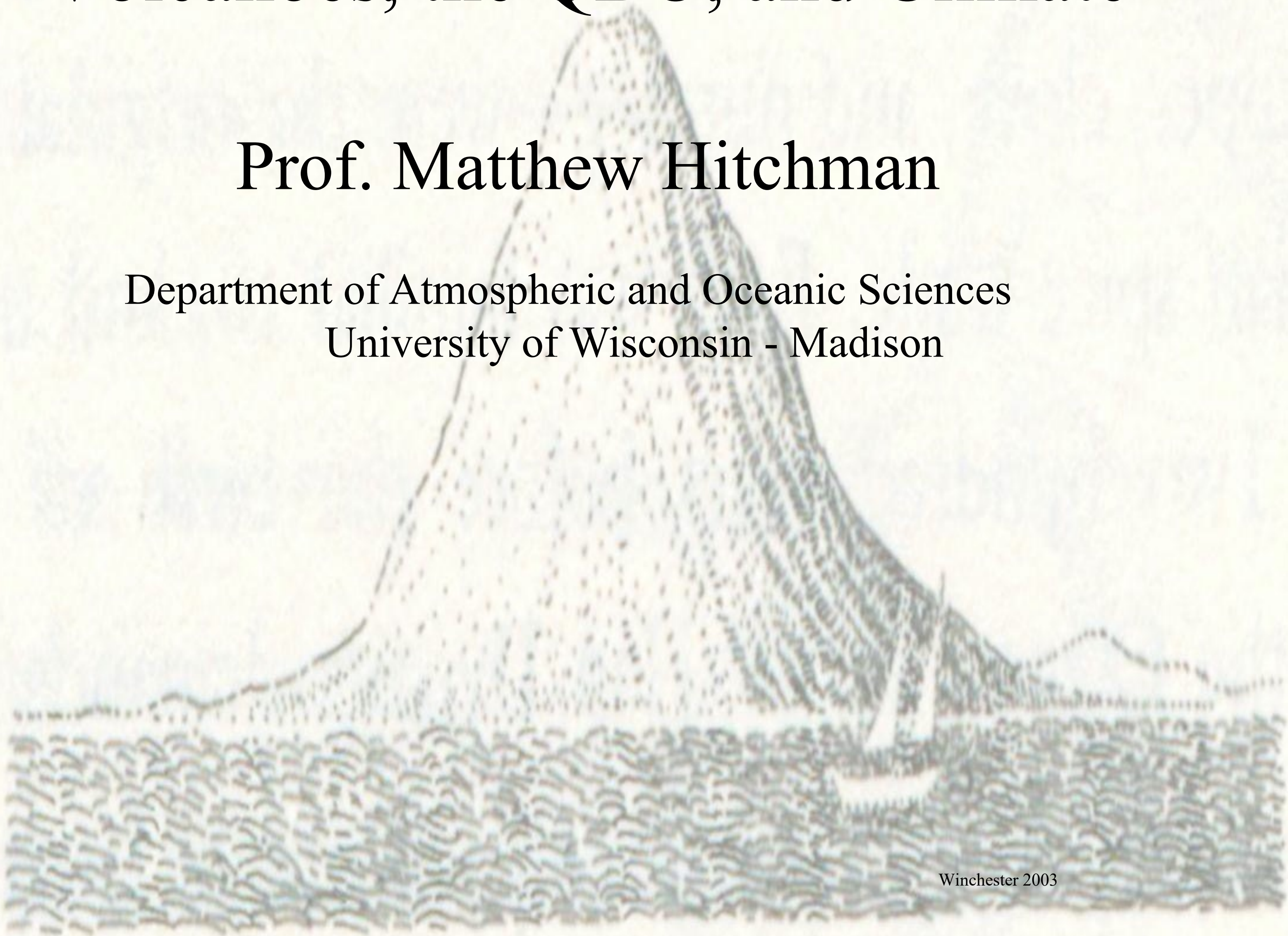

Winchester 2003

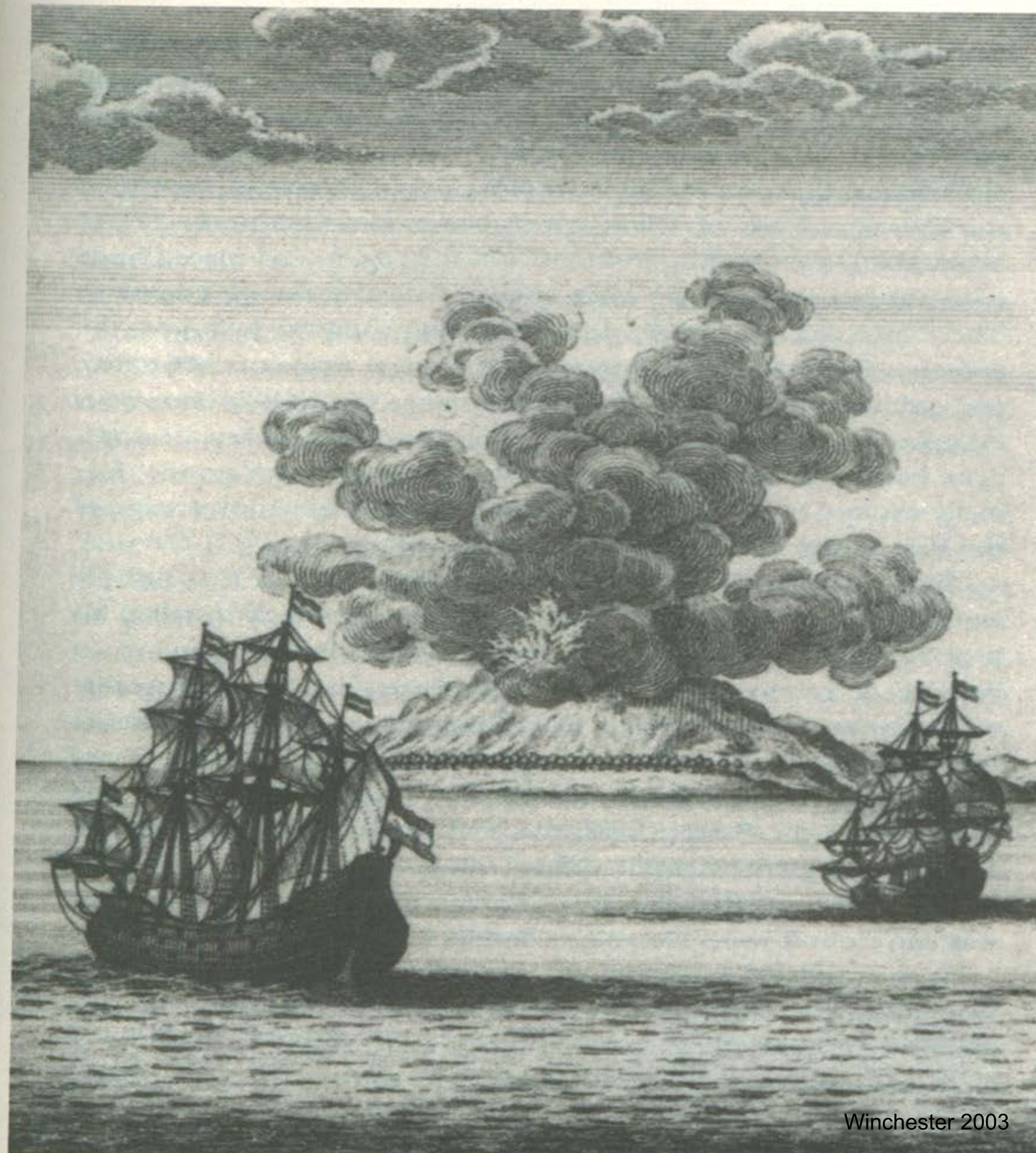

Jan van Schley's early etching *Het Brandende Eiland*, showing two caravels passing in front of what is presumed to be Krakatoa in full eruption, in what is further presumed to be 1680.

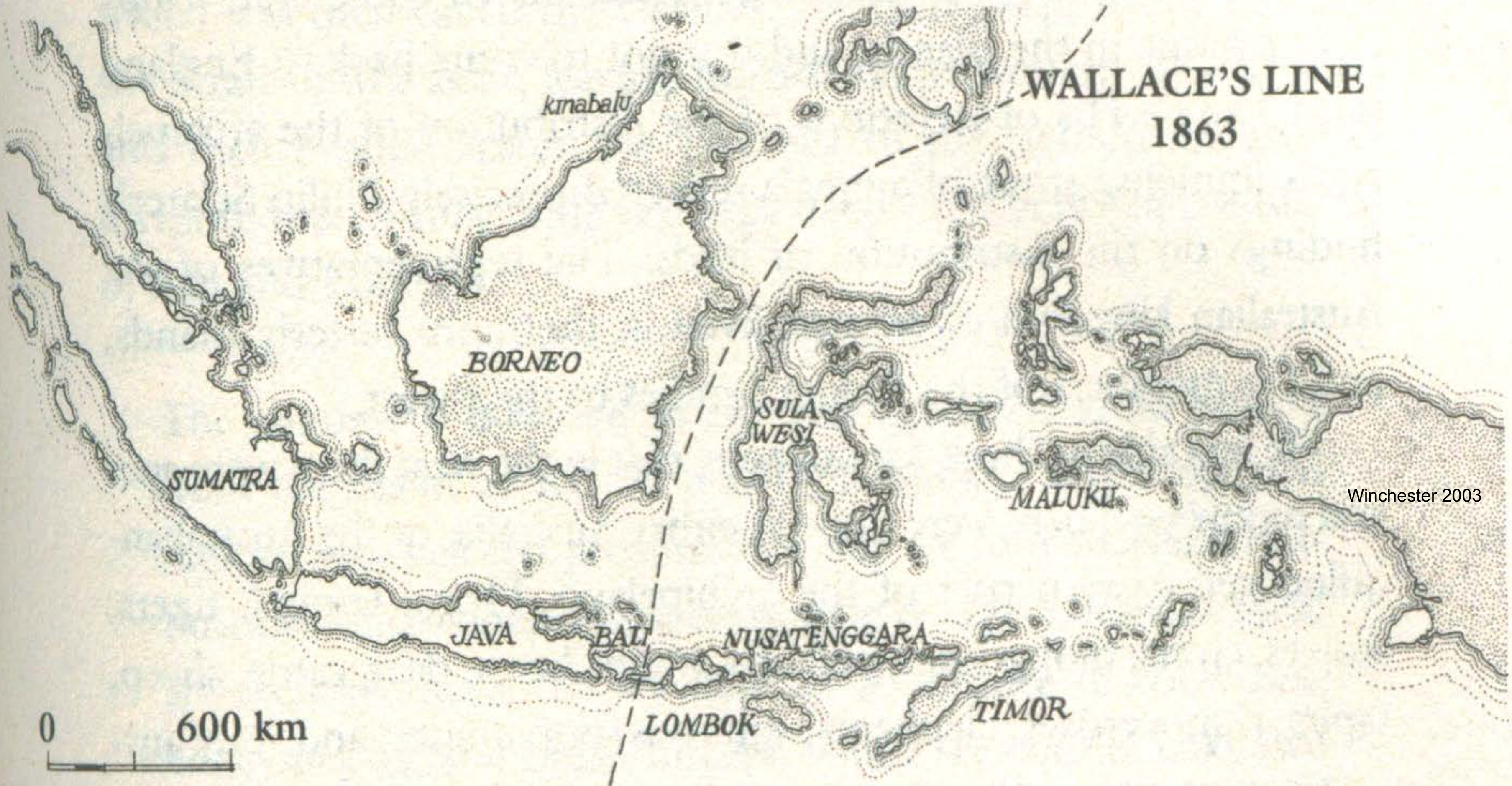

The Wallace Line—Australian fauna (cockatoos, kangaroos) to its east, Indo-European thrushes, monkeys, and deer to its west.

Krakatoa August 27, 1883

Winchester 2003

The Royal Dutch Navy's armed paddle steamer *Berouw* about to be picked up by one of the giant tsunamis generated by the eruption.

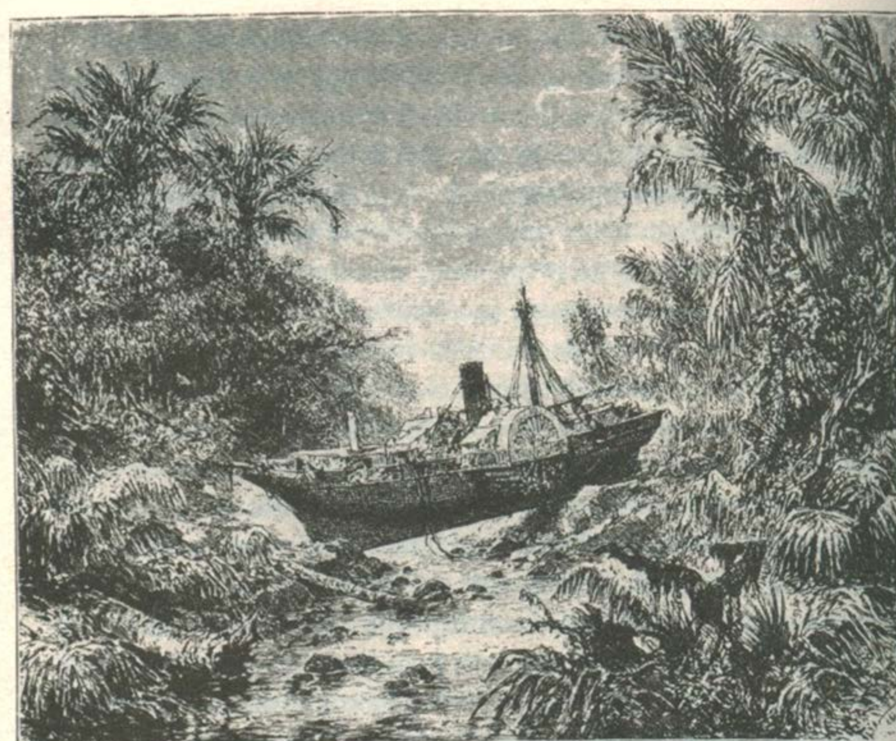

The *Berouw*, well and truly stranded—but very little damaged—a mile and a half up the Koeripan River. Hunks of rusting iron remained in the jungle until the 1980s.

Winchester 2003

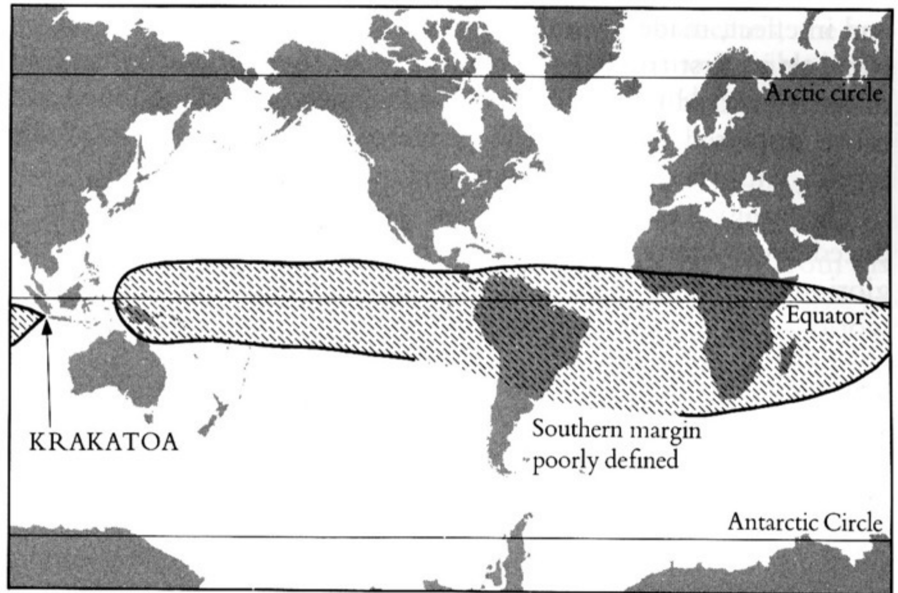

7 September 1883

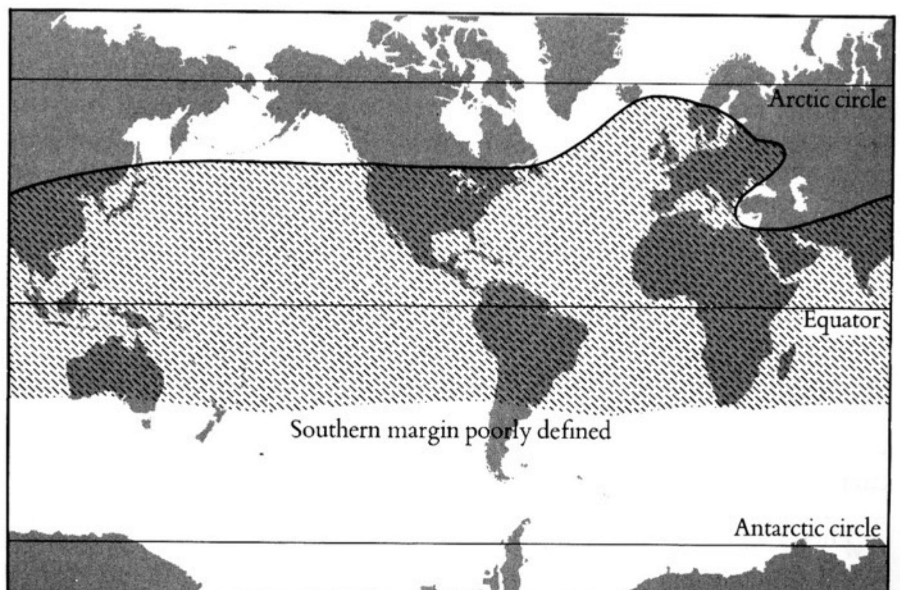

30 November 1883

Fig. 65 Two maps from the Royal Society report on the Krakatoa eruption, showing the westward drift of the ash cloud and its spread northwards.

Plate 4. Sunset over Lake Mendota in Madison, Wisconsin, in May 1983, one year after the El Chichón eruption. Photograph by A. Robock.

Ergebnisse der Arbeiten
des Königlich Preußischen Aeronautischen Observatoriums bei Lindenberg
herausgegeben durch dessen Direktor Dr. Richard Assmann

Bericht über die aerologische Expedition
des
Königlichen Aeronautischen Observatoriums
nach Ostafrika im Jahre 1908

erstattet von ihrem Leiter

Arthur Berson

Mit 13 in den Text gedruckten Abbildungen und 21 Tafeln

Braunschweig
Druck von Friedrich Vieweg und Sohn
1910

Preis 10 Mark.

26 August 1908 Shirati (1.08S, 33.59E)

Windverteilung.

Seehöhe m	Wind Richtung	Wind Geschwindigkeit m p. s.
1140	E	—
1140 — 2180	N 61° E	2.2
2180 — 2310	N 56 E	4.0
2310 — 2570	N 9 W	0.9
2570 — 2830	N 57 W	1.1
2830 — 3210	S 49 W	2.3
3210 — 3470	N 81 W	1.3
3470 — 3600	N 37 W	3.4
3600 — 3860	N 3 W	1.9
3860 — 4120	N 86 E	1.0
4120 — 4380	S 45 E	3.4
4380 — 4630	S 8 E	3.6
4630 — 4890	S 32 E	7.1
4890 — 5410	S 59 E	6.7
5410 — 6180	S 54 E	8.4
6180 — 6700	S 53 E	10.2
6700 — 7210	S 57 E	13.4
7210 — 7730	S 65 E	9.0
7730 — 8250	S 61 E	5.2
8250 — 8760	S 58 E	4.1
8760 — 9280	S 49 E	5.9
9280 — 9790	S 47 E	6.2
9790 — 10310	S 33 E	7.8
10310 — 10830	S 49 E	8.9
10830 — 11340	S 55 E	7.9
11340 — 11730	S 46 E	6.6
11730 — 11990	S 15 W	4.8
11990 — 12500	S 40 W	2.6
12500 — 12760	N 89 W	2.1
12760 — 13530	N 49° W	5.3
13530 — 14000	N 5 W	4.8
14000 — 14570	N 27 E	9.0
14570 — 15080	N 61 E	12.4
15080 — 15730	N 74 E	20.6
15730 — 15990	N 68 E	24.5
15990 — 16240	N 74 E	25.4
16240 — 16500	N 78 E	34.3
16500 — 16760	N 85 E	26.7
16760 — 17020	S 86 E	20.4
17020 — 17280	S 77 E	17.1
17280 — 17790	S 68 E	9.9
17790 — 18050	S 57 E	13.0
18050 — 18310	S 69 E	8.4
18310 — 18440	S 78 E	3.2
18440 — 18690	N	1.6
18690 — 19210	S 59 W	3.2
19210 — 19470	N 82 W	4.6
	ein Ballon geplatzt	
Abstieg		
19470 — 18670	S 83 W	5.2
18670 — 17140	S 60 E	6.2
17140 — 16030	N 86 E	21.1
16030 — 14680	N 66 E	17.9
14680 — 13550	N 22 E	5.1
13550 — 12780	N 47 W	7.0
12780 — 12160	NNW	1.4
12160 — 10770	SE	1.3
	verschwunden	

The Quasibiennial Oscillation

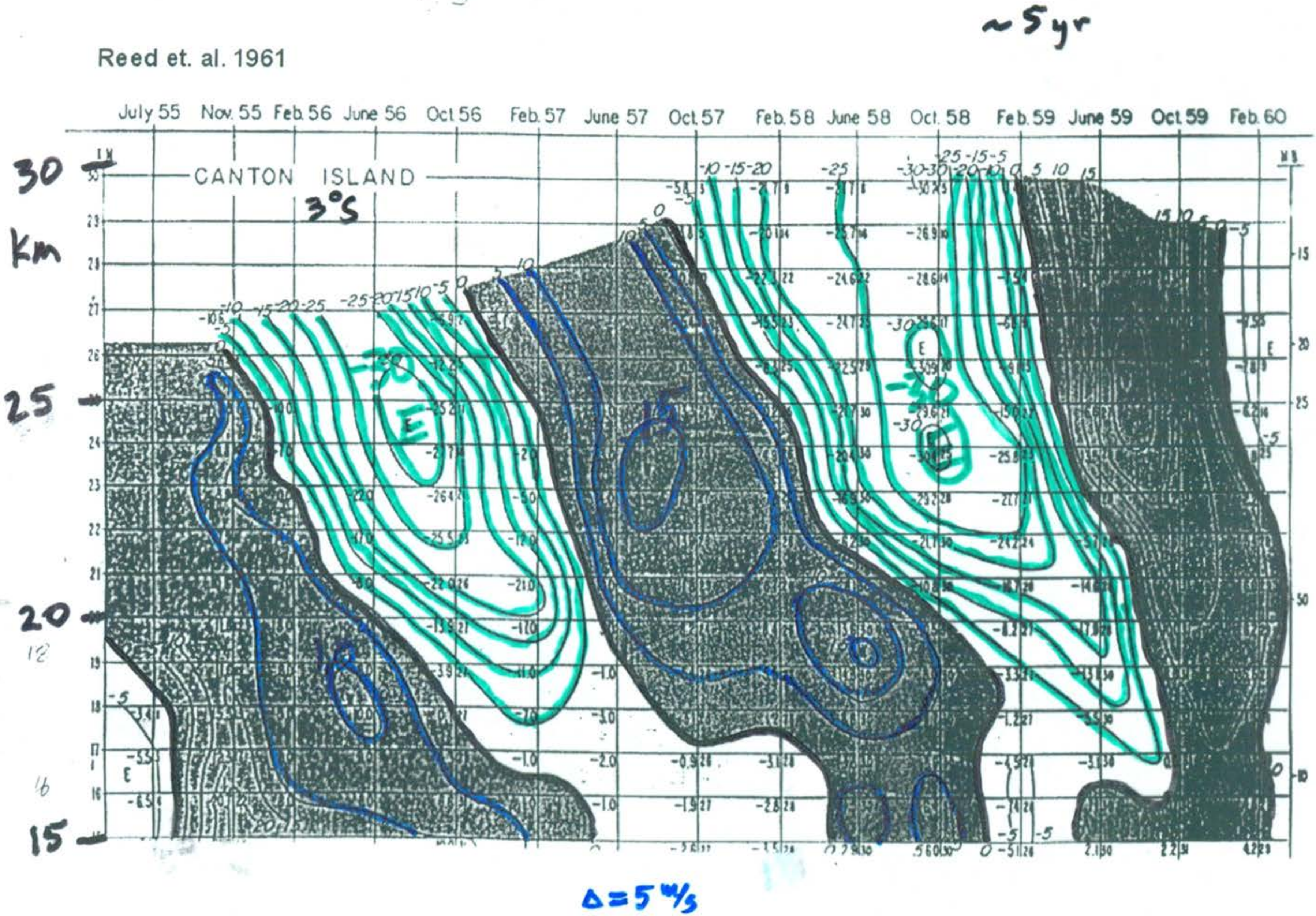

Trepte (1993)

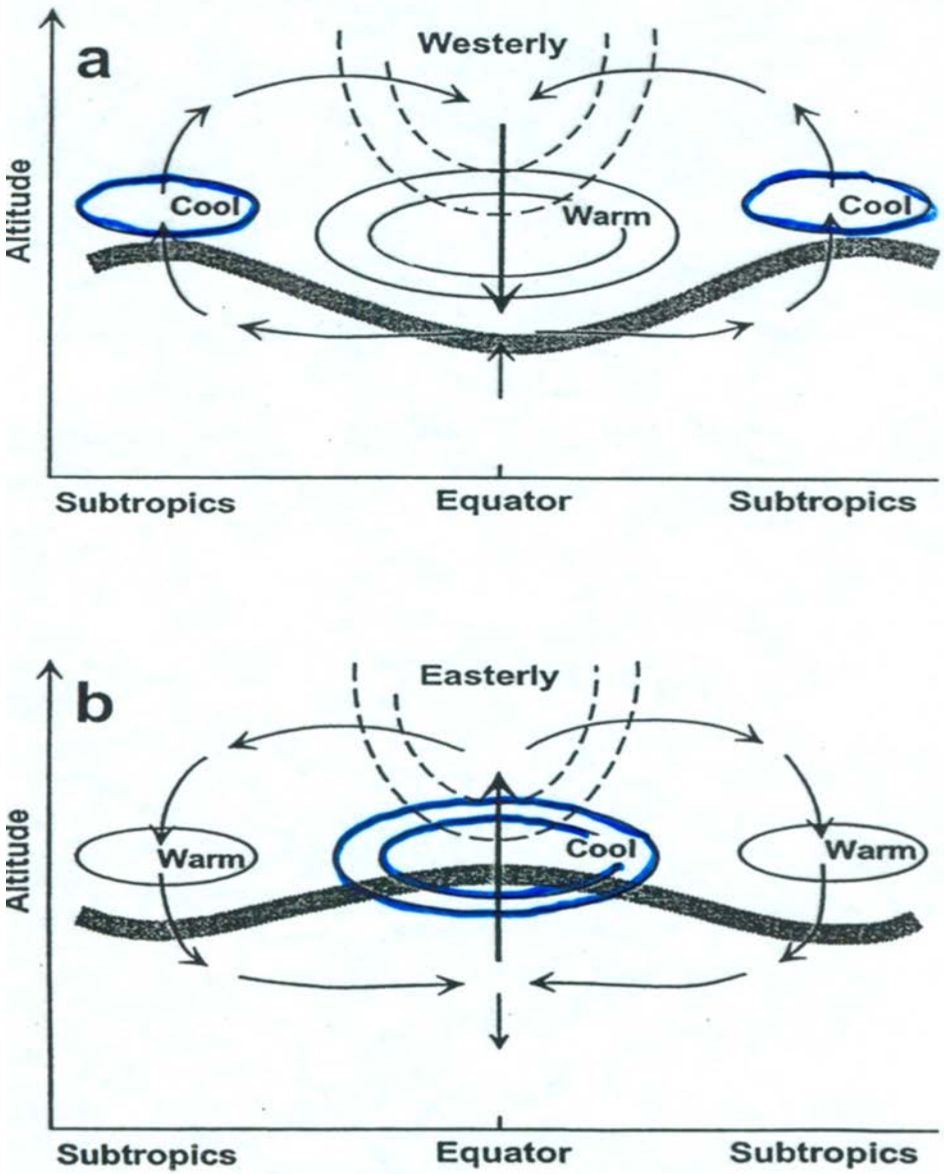

a
Westerly
Cool
Warm
Cool
Altitude
Subtropics
Equator
Subtropics
b
Easterly
Warm
Cool
Warm
Altitude
Subtropics
Equator
Subtropics

TABLE 1. Volcanoes in the Period 1850–1991 of Severity Class 2 or Higher

Sato et al. (1993) JGR

Date	Volcano	Latitude, Longitude	Severity	VEI
1854, Feb.	Sheveluch, Kamchatka	57°N, 162°E	···	5
1855–1856	Cotopaxi, Ecuador	1°S, 78°W	1.5	···
1856, Feb.	Awu, Celebes	4°N, 125°E	2	···
1861, Dec.	Makjan, Molucca Islands	0°N, 127°E	2	4
1875, March	Askja, Iceland	65°N, 17°W	2	5
1883, Aug.	Krakatau, Indonesia	6°S, 105°E	1	6
1886, June	Tarawera, New Zealand	38°S, 177°E	2	5
1888, March	Ritter Island, Bismarck Archipelago	6°S, 148°E	2	···
1888, July	Bandai San, Japan	38°N, 140°E	2	4
1892, June	Awu, Celebes	4°N, 125°E	2	···
1902, May	Mont Pelée, Martinique	15°N, 61°W	2	4
1902, May	Soufrière, St. Vincent	13°N, 61°W	2	4
1902–1904	Santa Maria, Guatemala	15°N, 92°W	1.33	5–6
1907, March	Shtyubelya, Kamchatka	52°N, 158°E	2	5
1912, June	Katmai, Alaska	58°N, 155°W	2	6
1932, April	Quizapu, Cerro Azul	36°S, 71°W	3	5
1947, March	Hekla, Iceland	64°N, 20°W	2	4
1953, July	Mount Spurr, Alaska	61°N, 152°W	2	4
1956, March	Bezymyannaya, Kamchatka	56°N, 161°E	2	5
1963, March	Gunung Agung, Bali	8°S, 116°E	1.5	4
1966, Aug.	Awu, Celebes	4°N, 125°E	2	4
1968, June	Fernandina Island, Galapagos	0°S, 92°W	2	4
1980, May	St. Helens, United States	46°N, 122°W	···	5
1982, April	El Chichon, Mexico	17°N, 93°W	···	5
1991, June	Pinatubo, Philippines	15°N, 120°E	···	5
1991, Aug.	Hudson, Chile	46°S, 73°W	···	5

The severity numbers 1, 2, 3 of *Mitchell* [1970] are intended by the author to represent volumes of ejecta 1–10, 0.1–1, 0.01–0.1 km^3, respectively. Volcanic explosivity index (VEI) numbers 6, 5, 4 of *Newhall and Self* [1982] are intended by the authors to represent volumes of ejecta 10–100, 1–10, 0.1–1 km^3, respectively.

Sato et al. (1993) JGR

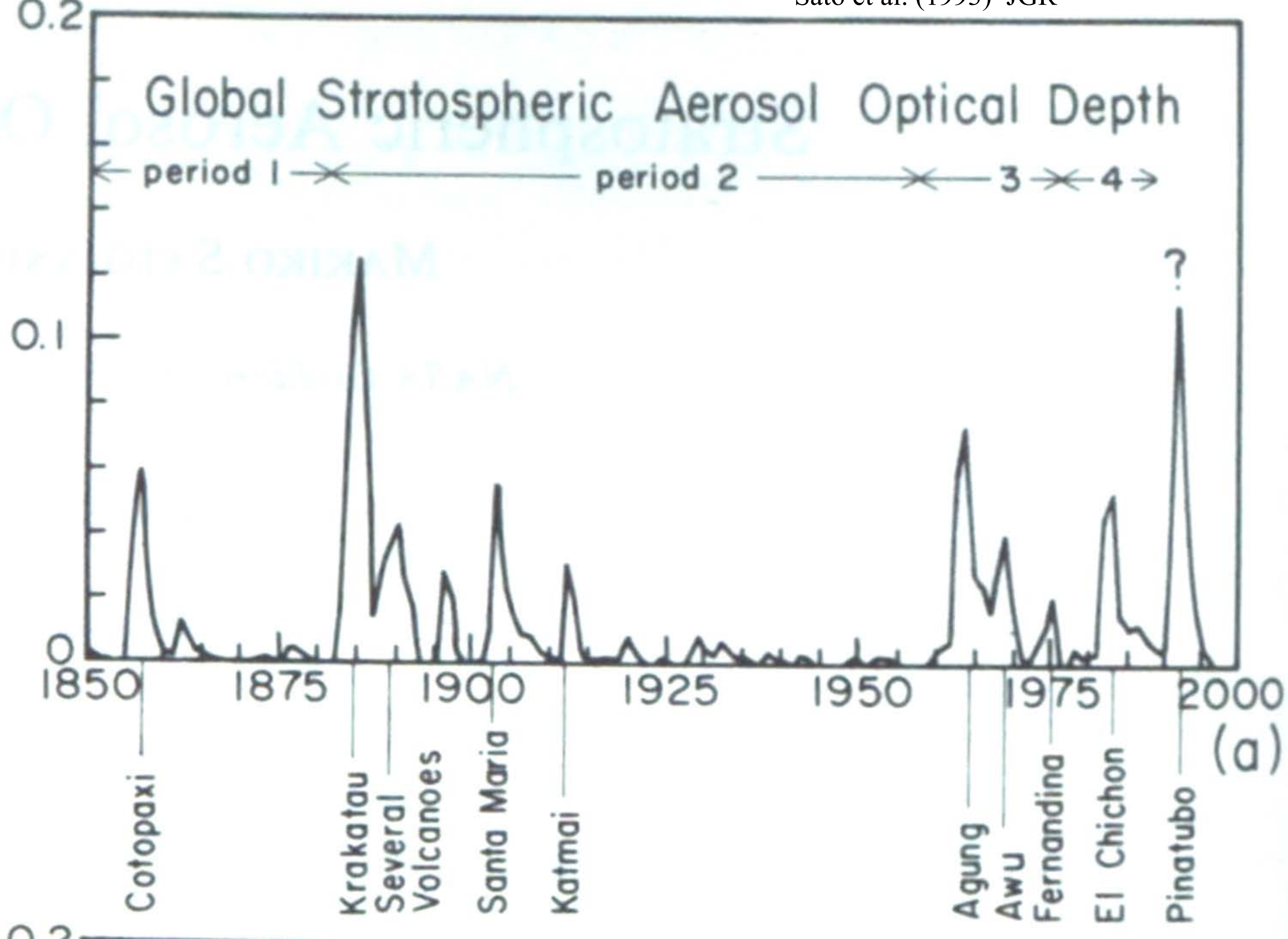

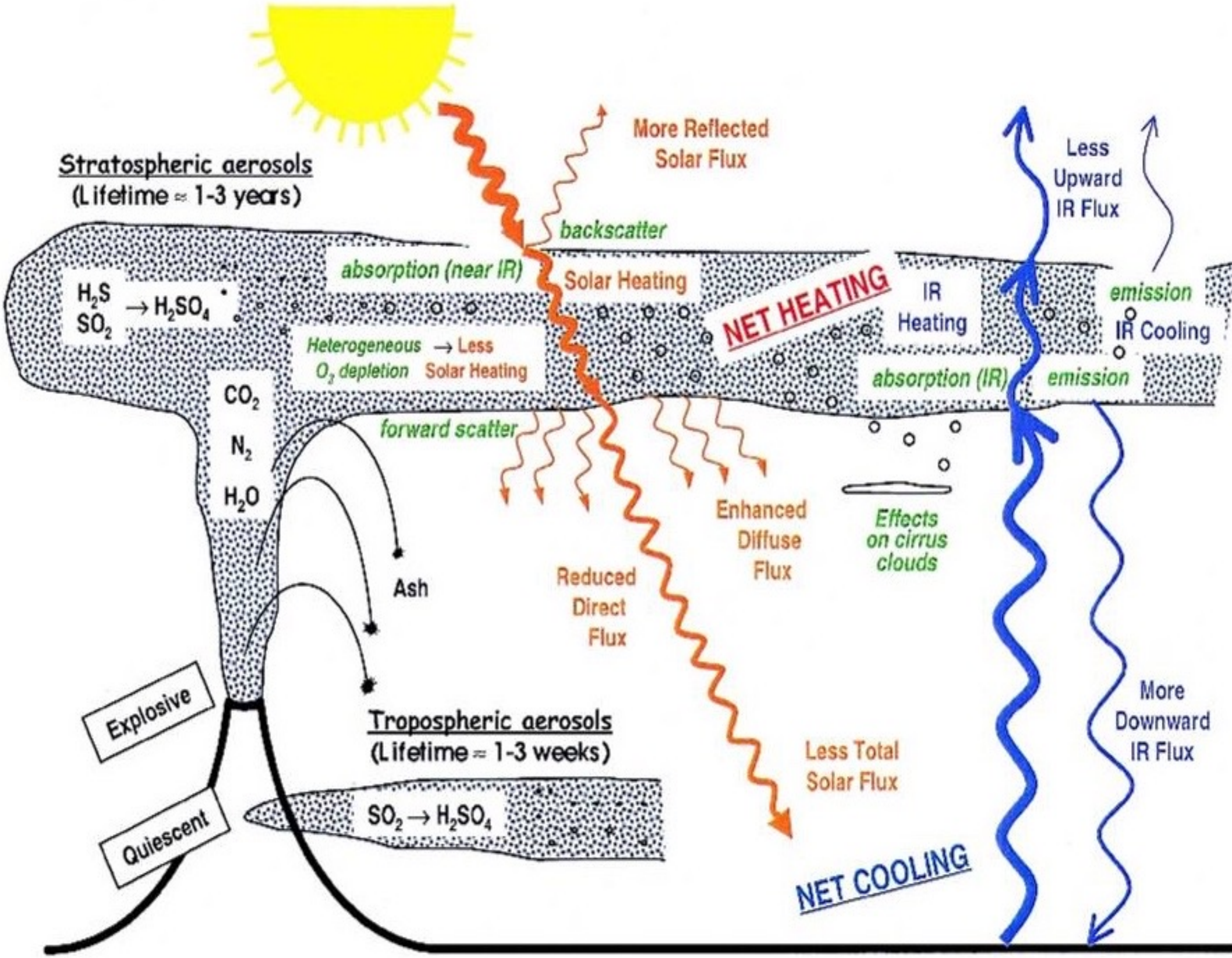

Plate 1. Schematic diagram of volcanic inputs to the atmosphere and their effects. This is an extended version of Figures 1 and 2 of *Simarski* [1992], drawn by L. Walter and R. Turco.

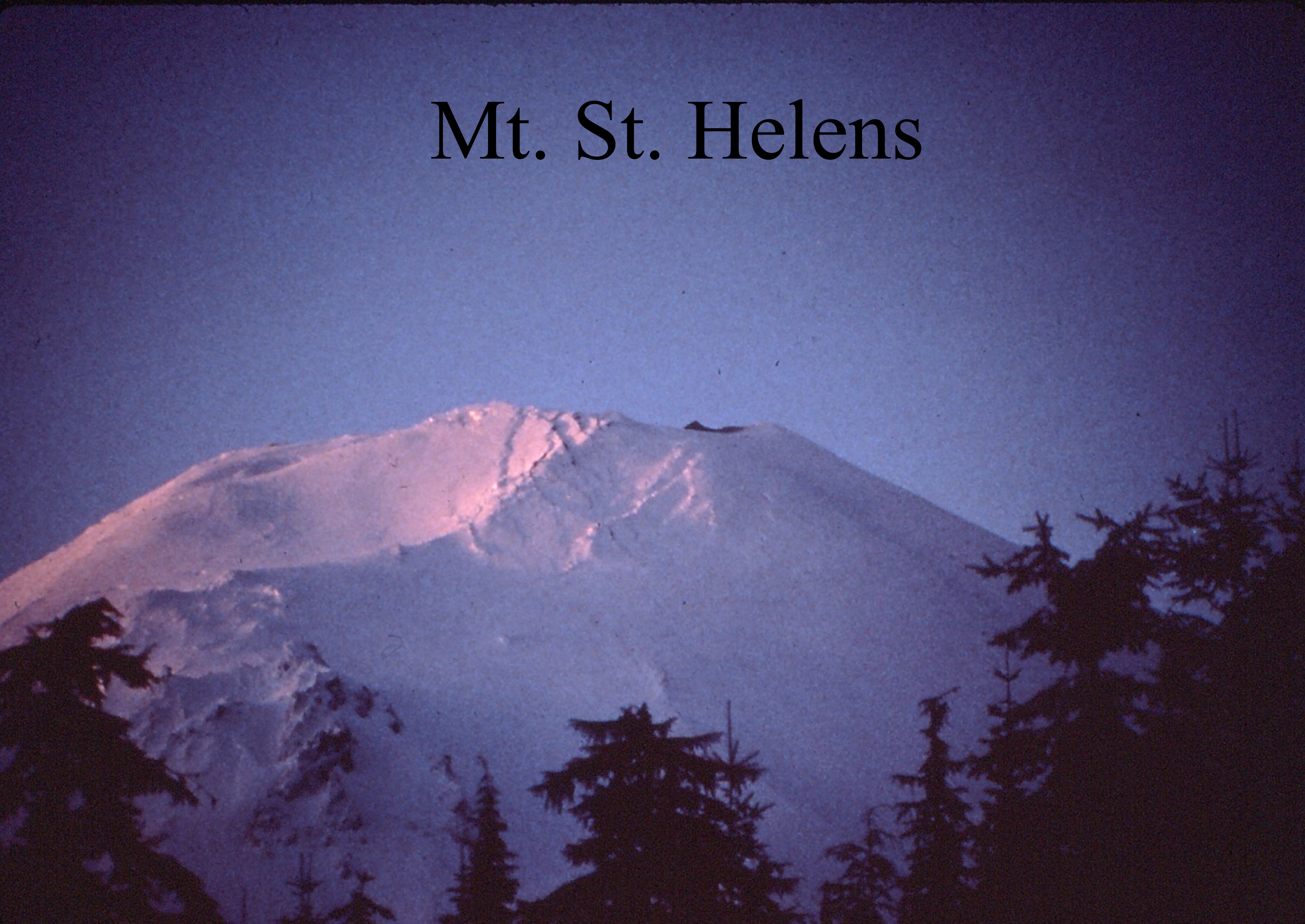
Mt. St. Helens


18 May 1980

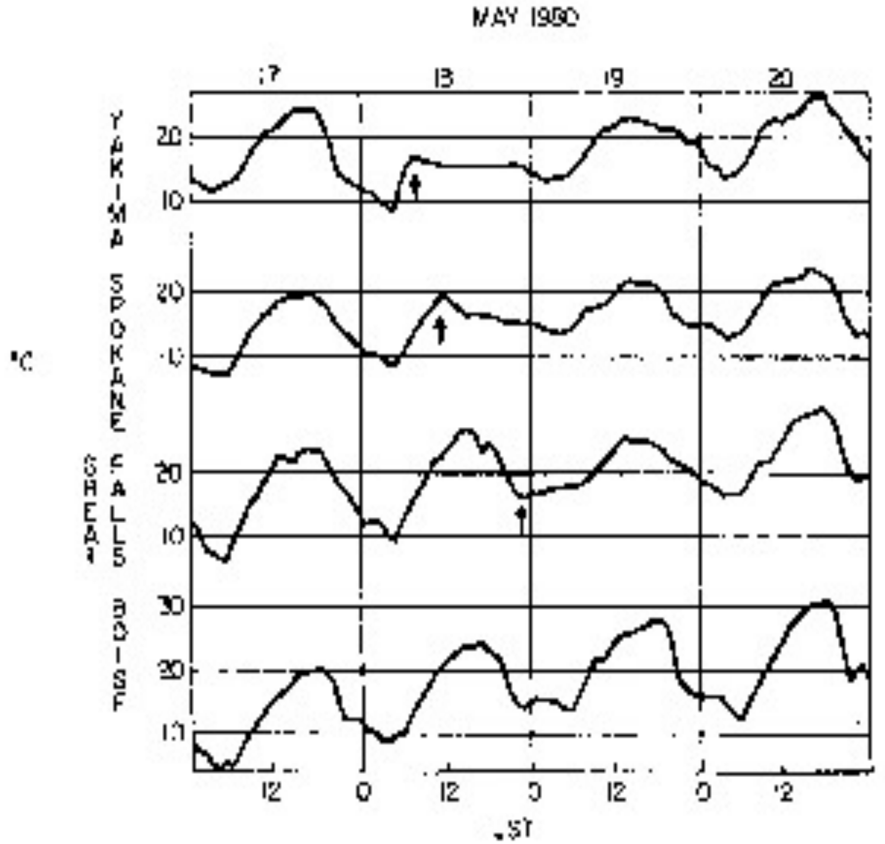

Figure 3. Time series of surface air temperature for Yakima and Spokane, Washington; Great Falls, Montana; and Boise, Idaho, for May 17–20, 1980, under the plume of the 1980 Mount St. Helens eruption, from Figure 3 of *Robock and Mass* [1982]. Time of arrival of the plume is indicated with an arrow. LST is local standard time. The plume never passed over Boise, which is included as a control. Note the damping of the diurnal cycle after the arrival of the tropospheric aerosol cloud.

Mount St. Helens, Washington, ash and gas emission, May 16, 1983; view to S. Photo by Patrick Pringle.

SAGE I / SAGE II / SAM II Aerosol Climatology

- Quasi-biennial Oscillation
- Brewer-Dobson Circulation
- Annual cycle
- Tropical reservoir
- Lower and upper transport regimes
- Transport pathways of aerosol out of the tropics into extratropical anticyclones

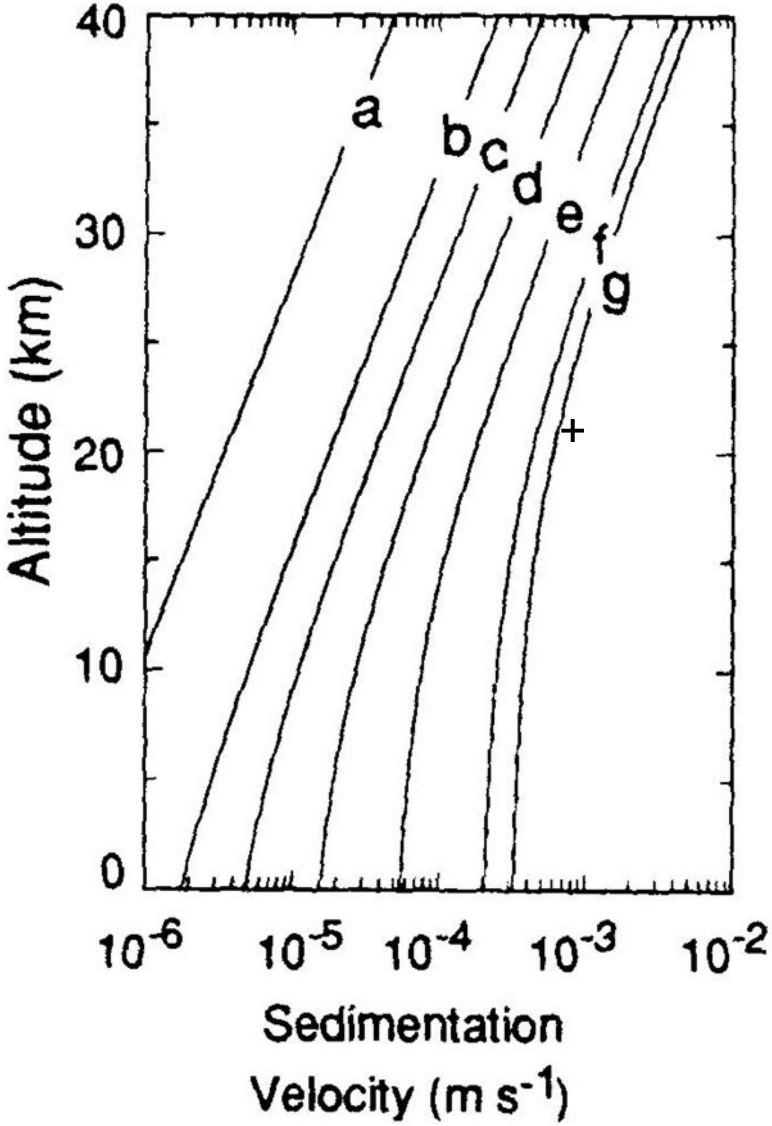

Sed Vel ~ w* QBO < 1 mm/s

Trepte (1993)

Fig. 2.10. Particle terminal velocities computed for typical tropical conditions for particles with radii of a) 0.01 µm, b) 0.05 µm, c) 0.1 µm, d) 0.2 µm, e) 0.4 µm, f) 0.8 µm, and g) 1.0 µm.

SAGE II Extinction ratio

Trepte and Hitchman Nature (1992)

November 1984

October 1988

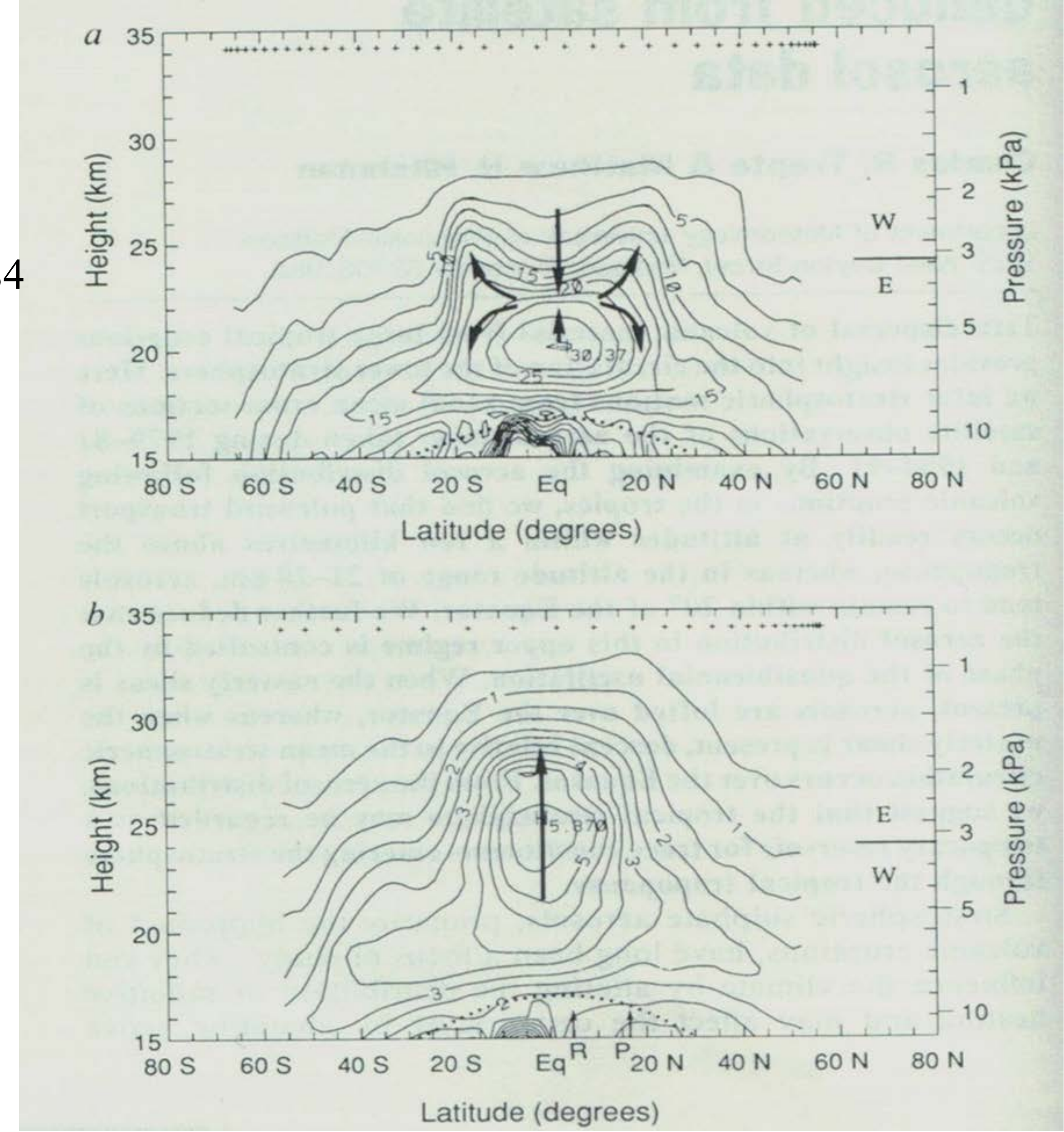

(1994)

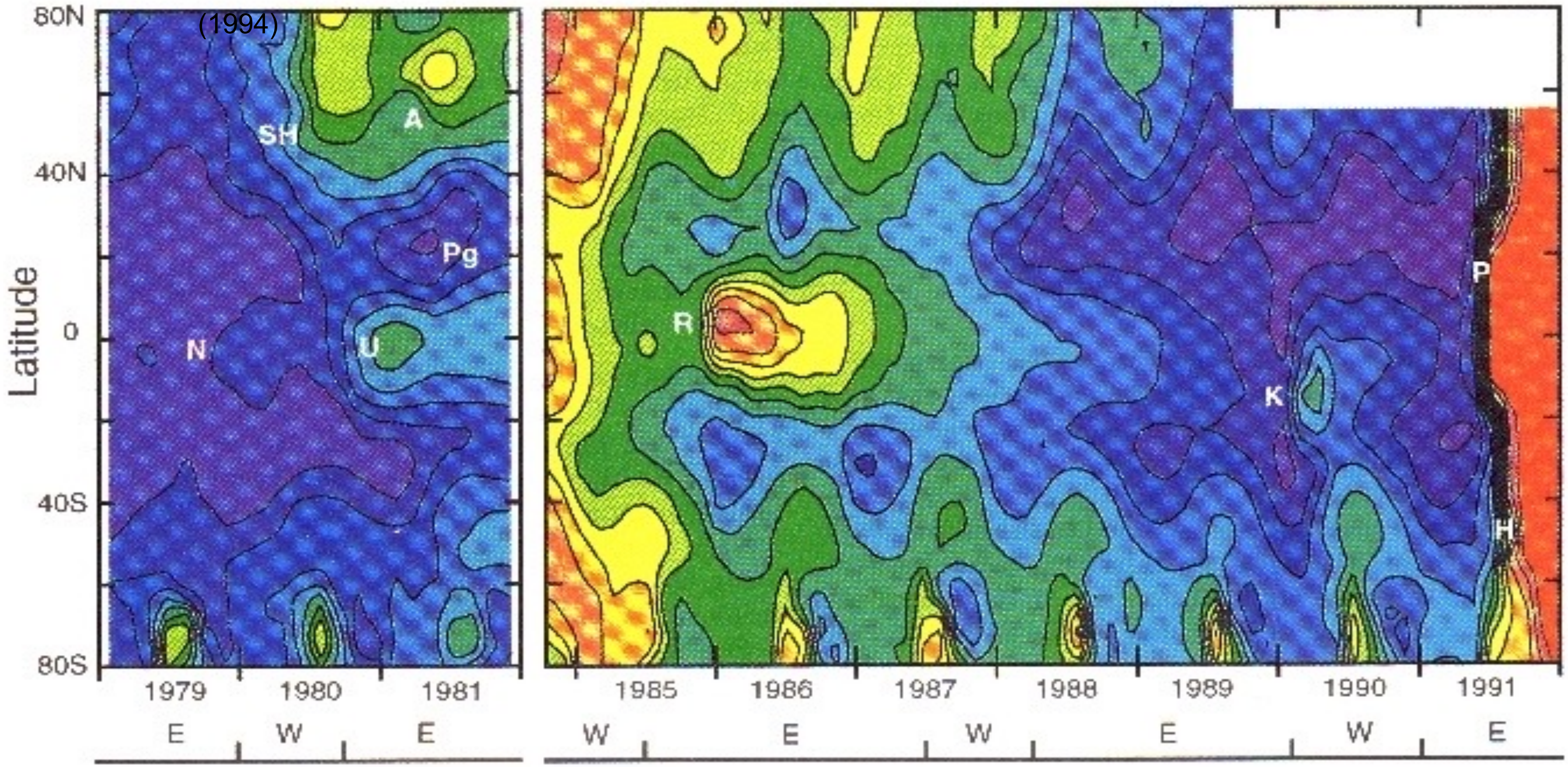

Plate 1. Time-latitude section of stratospheric aerosol optical depth at 1 μm, blending SAGE I and II and SAM II data. The logarithm of optical depth is shaded for values less than -2.9 to greater than -1.7, with color change at interval 0.1. Letters indicate specific volcanic eruptions (see text). The dominant phase of the QBO is indicated below the time line, where W (E) indicates westerly (easterly) shear. SAM II data in the northern polar latitudes are unavailable after late 1989 because of gradual orbital precession.

Thomasen, Poole, and Deshler (1997) JGR

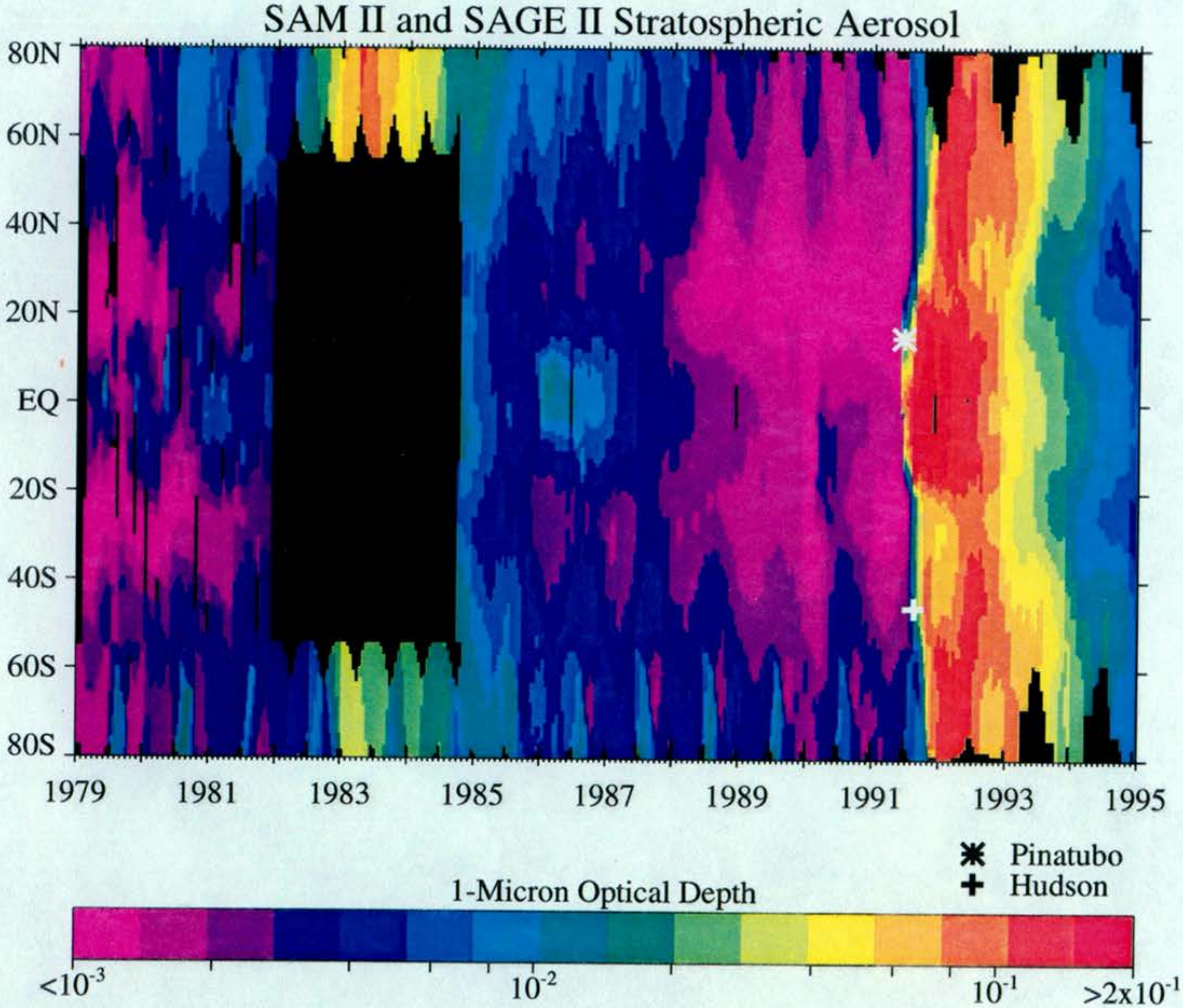

Figure 1. Stratospheric aerosol optical depth versus time and latitude derived from SAM II, SAGE, and SAGE II aerosol extinction profiles. Clear areas represent periods of no data availablilty.

Monthly Averaged Non-Rayleigh Backscatter Above Fritz Peak Observatory (40 °N, 105° W)

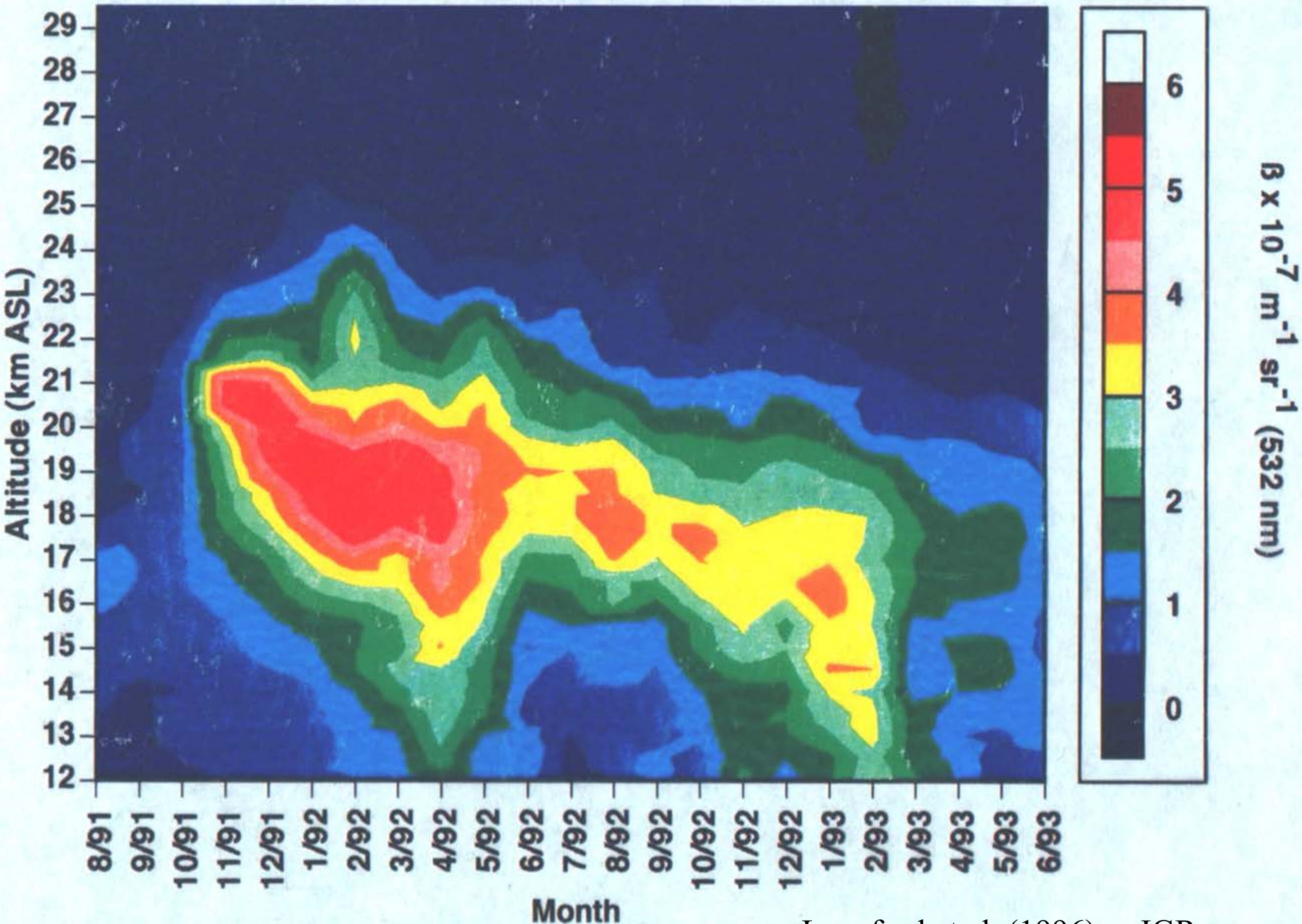

Langford et al. (1996) JGR

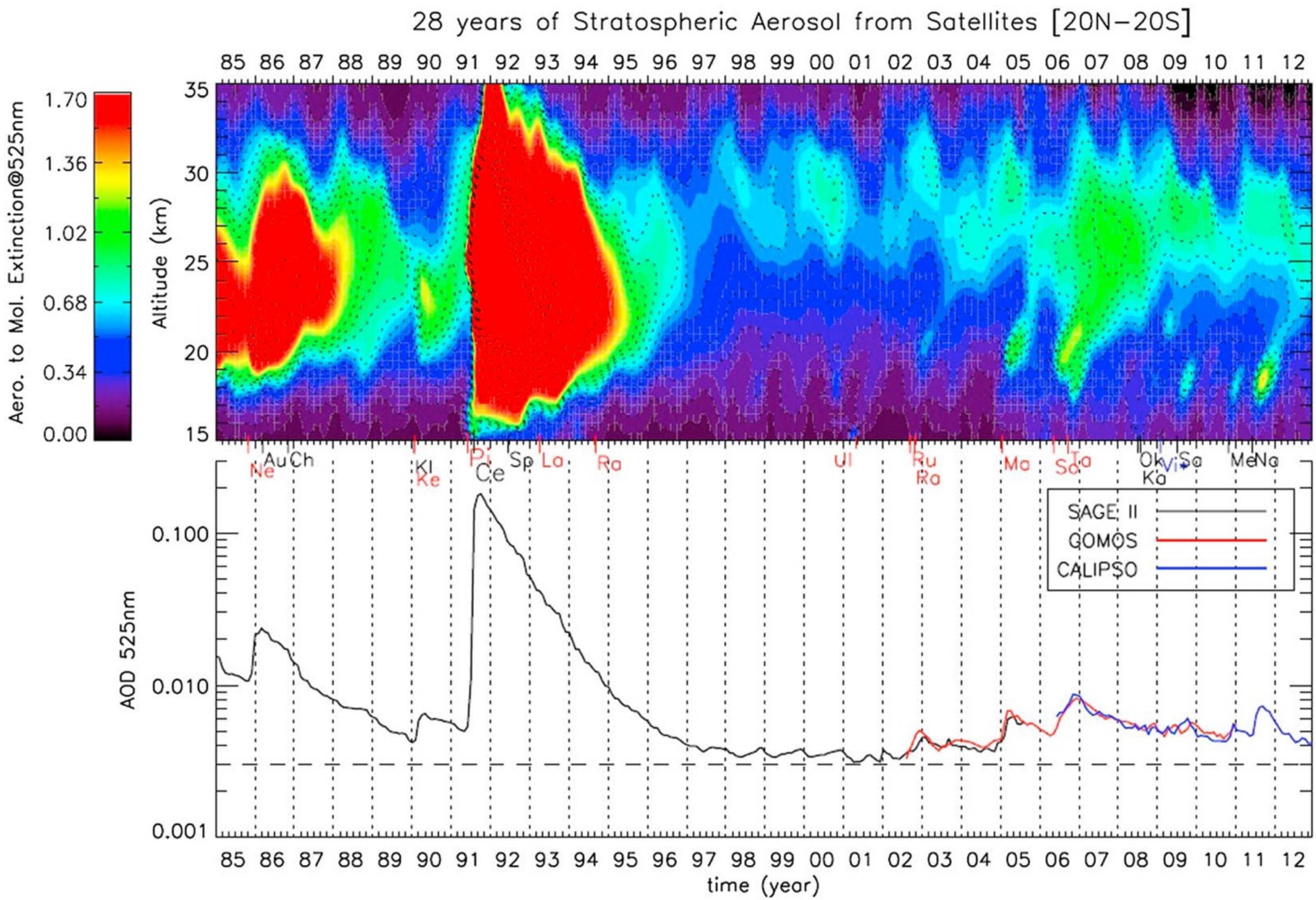

28 years of Stratospheric Aerosol from Satellites [20N-20S]
Aero. to Mol. Extinction@525nm
Altitude (km)
AOD 525nm
time (year)
SAGE II
GOMOS
CALIPSO
Ne
Au
Ch
Kl
Ke
Pi
Ce
Sp
La
Ra
Ul
Ru
Ra
Ma
So
Ta
Ok
Ka
Vi
Sa
Me
Na

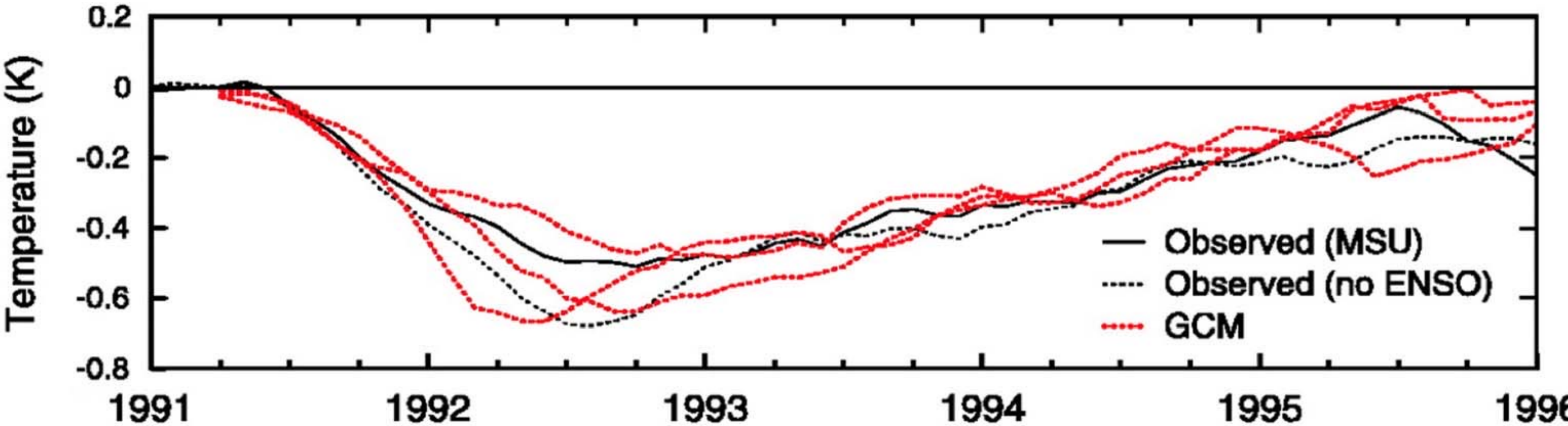

The observed (black lines) global-mean (90 °N–90 °S) changes in the lower tropospheric temperature compared to the modelled result (dashed red) after Mt. Pinatubo's eruption in June 1991.

From Soden et al., Science, 2002, 296, 727–730. Reprinted with permission from AAAS as Fig. 2 in H. N. Huynh and V. F. McNeill, 2024: The potential environmental and climate impacts of stratospheric aerosol injection: a review. *Environ. Sci.: Atmos.,* DOI: 10.1039/d3ea00134b.

Brewer-Dobson Circulation

9 year mean aerosol extinction ratio

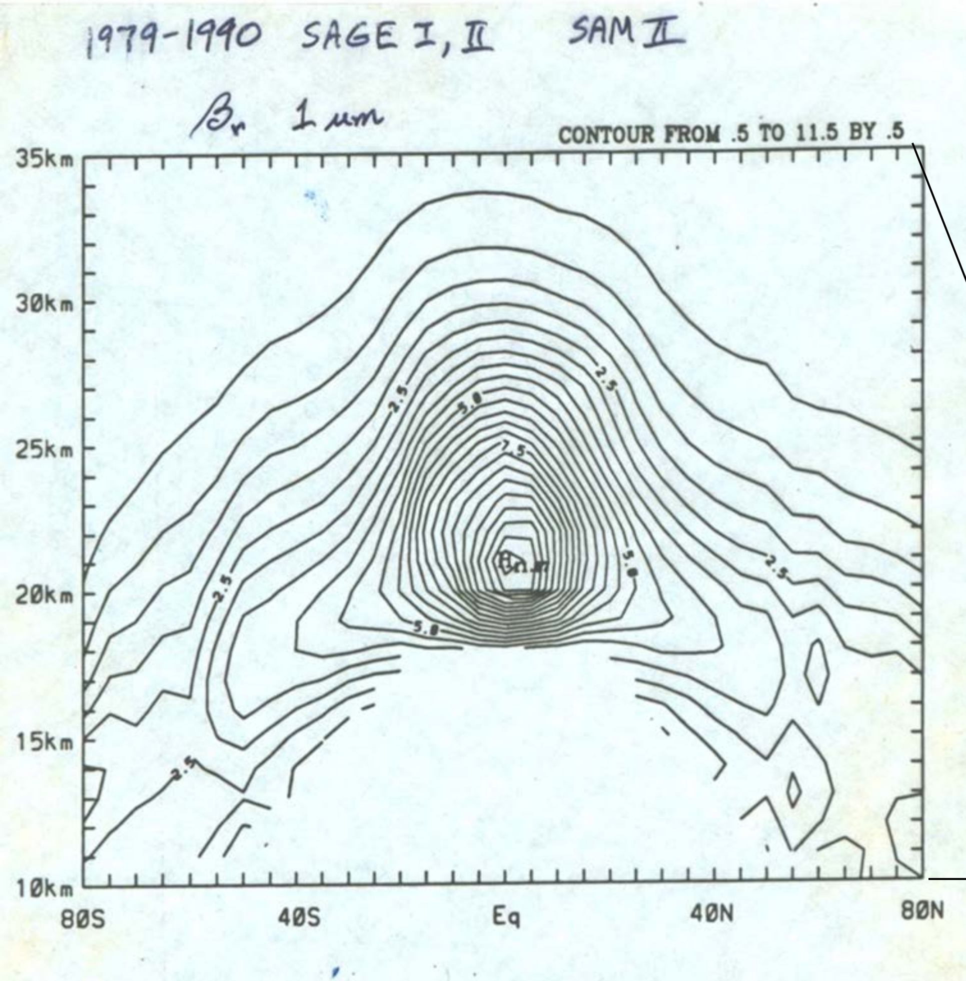

Hitchman et al. (1994) JGR

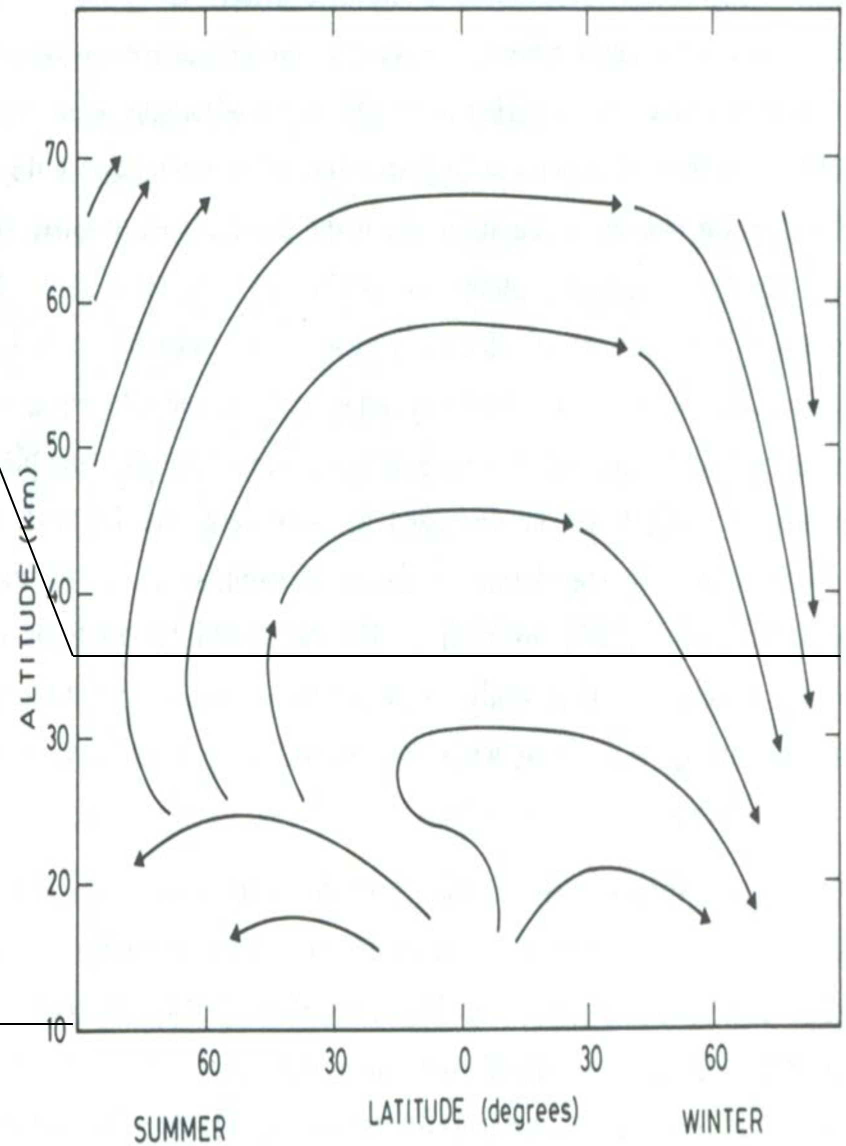

Murgatroyd and Singleton (1961) QJRMS
Dunkerton (1979) JAS

SAGE I SAGE II SAM II 1978-1991
5 QBO cycles

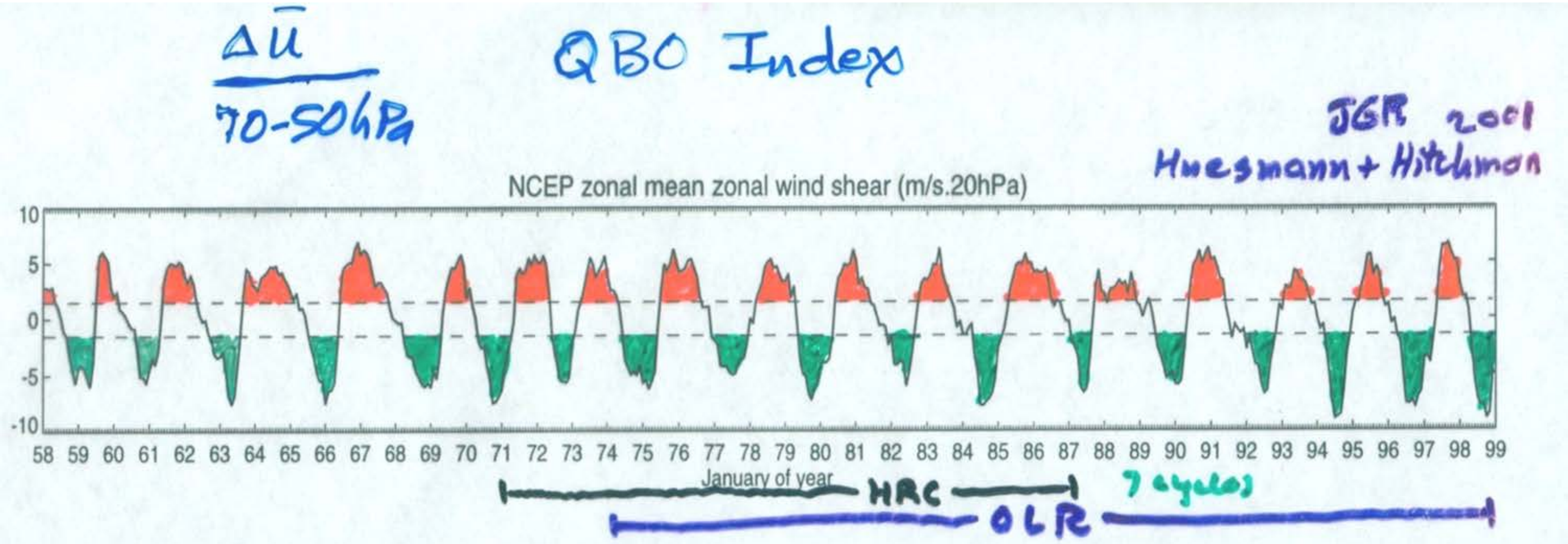

Trepte (1993)

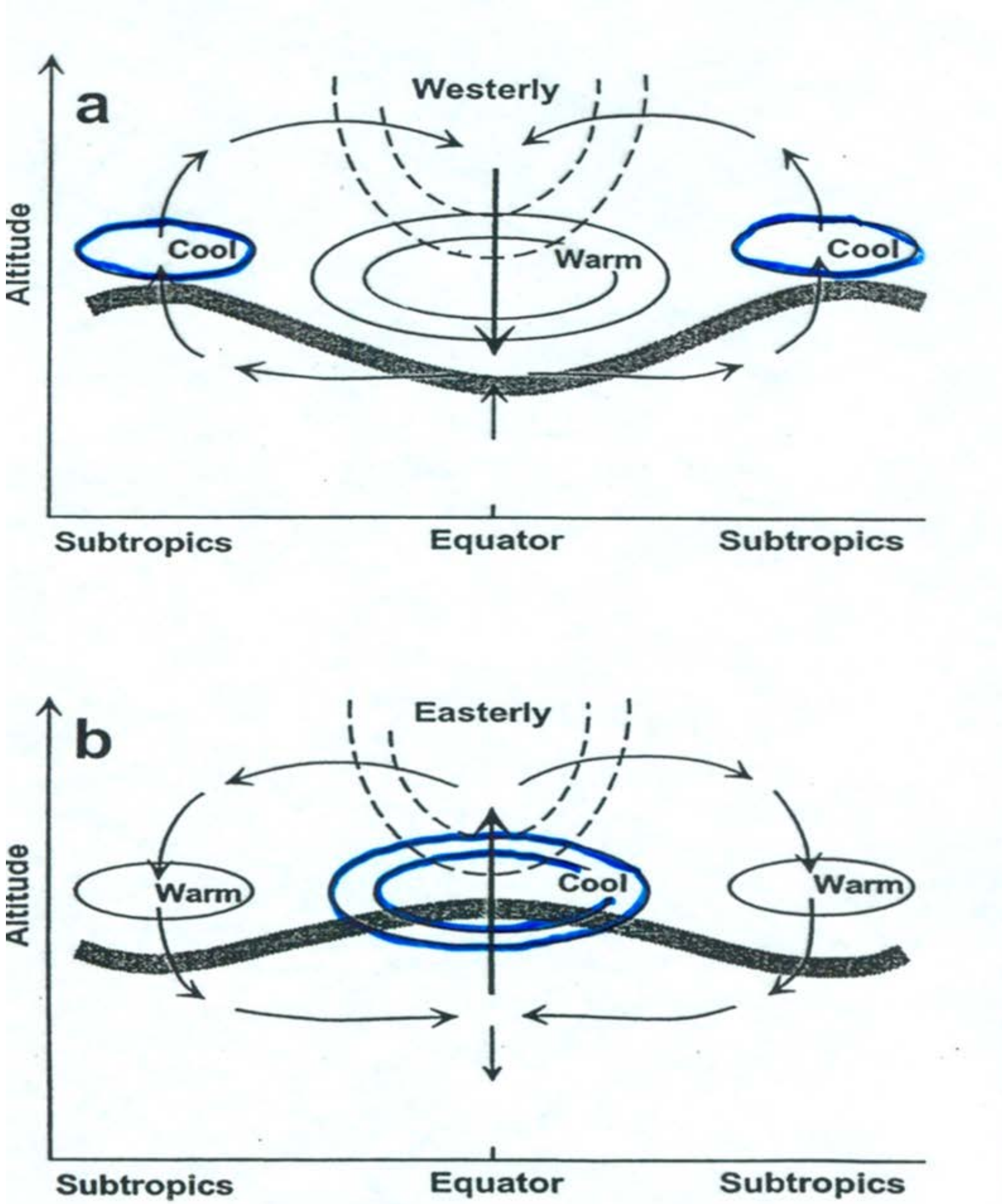

a
Westerly
Cool
Warm
Cool
Altitude
Subtropics
Equator
Subtropics
b
Easterly
Warm
Cool
Warm
Altitude
Subtropics
Equator
Subtropics

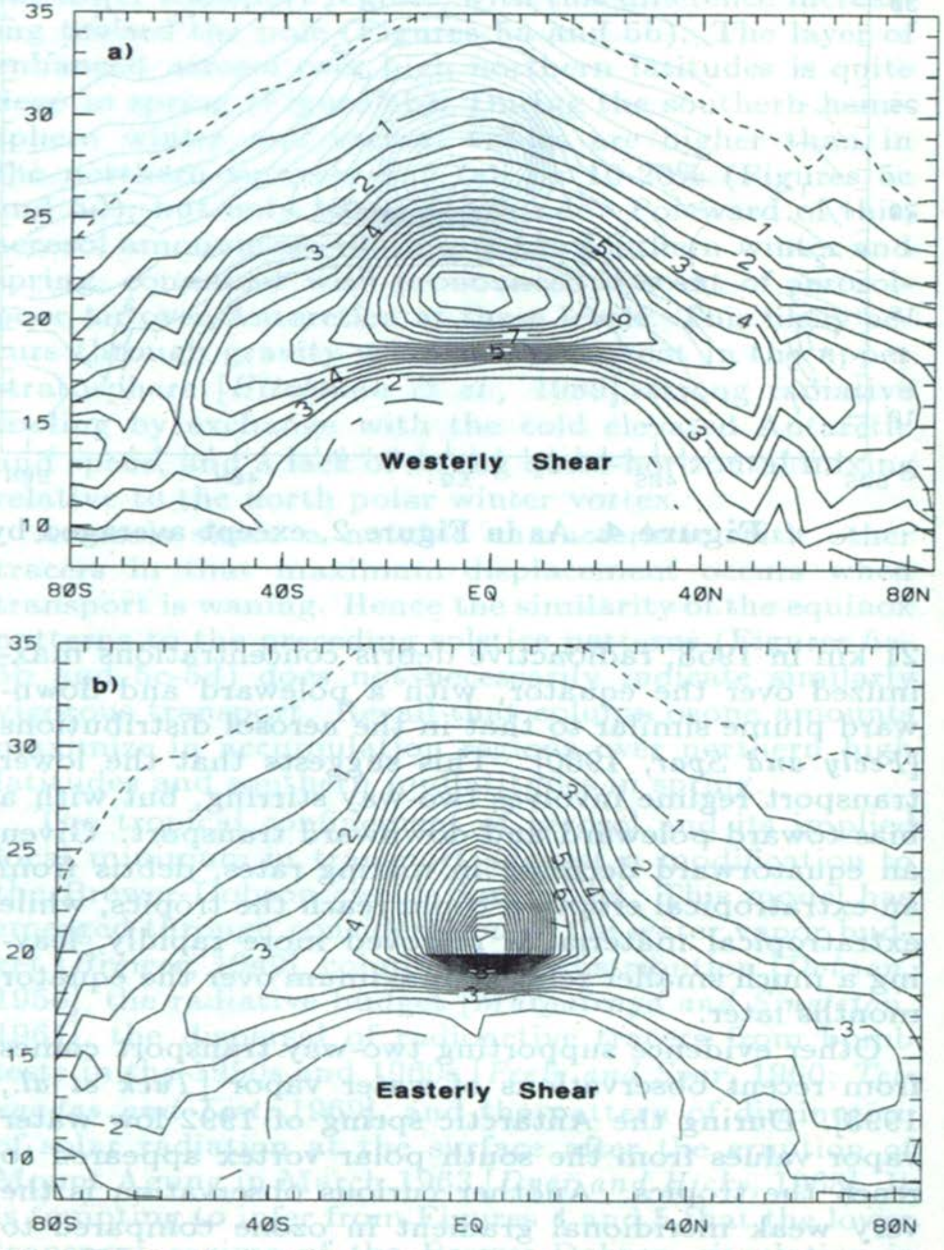

Figure 6. As in Figure 2, except averaged by phase of the QBO, as determined by predominant (a) westerly shear or (b) easterly shear of zonal wind at Singapore (see text).

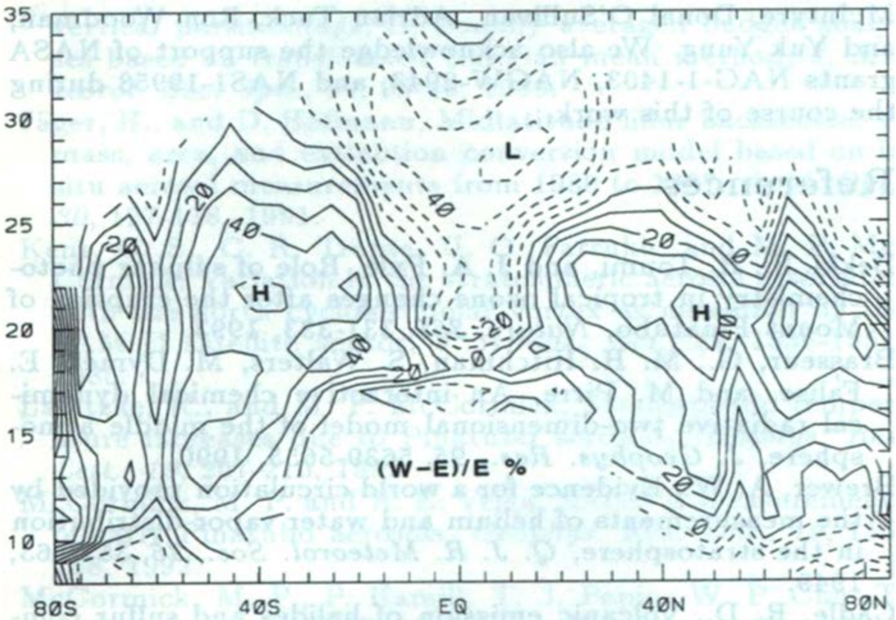

Figure 7. Latitude-altitude section of the percent difference in extinction ratio between the westerly shear and easterly shear phases of the QBO: (W - E)/W x 100, with contour interval 10%. Dashed contours indicate values which are higher during periods of predominant easterly shear.

Hitchman et al. (1994) JGR

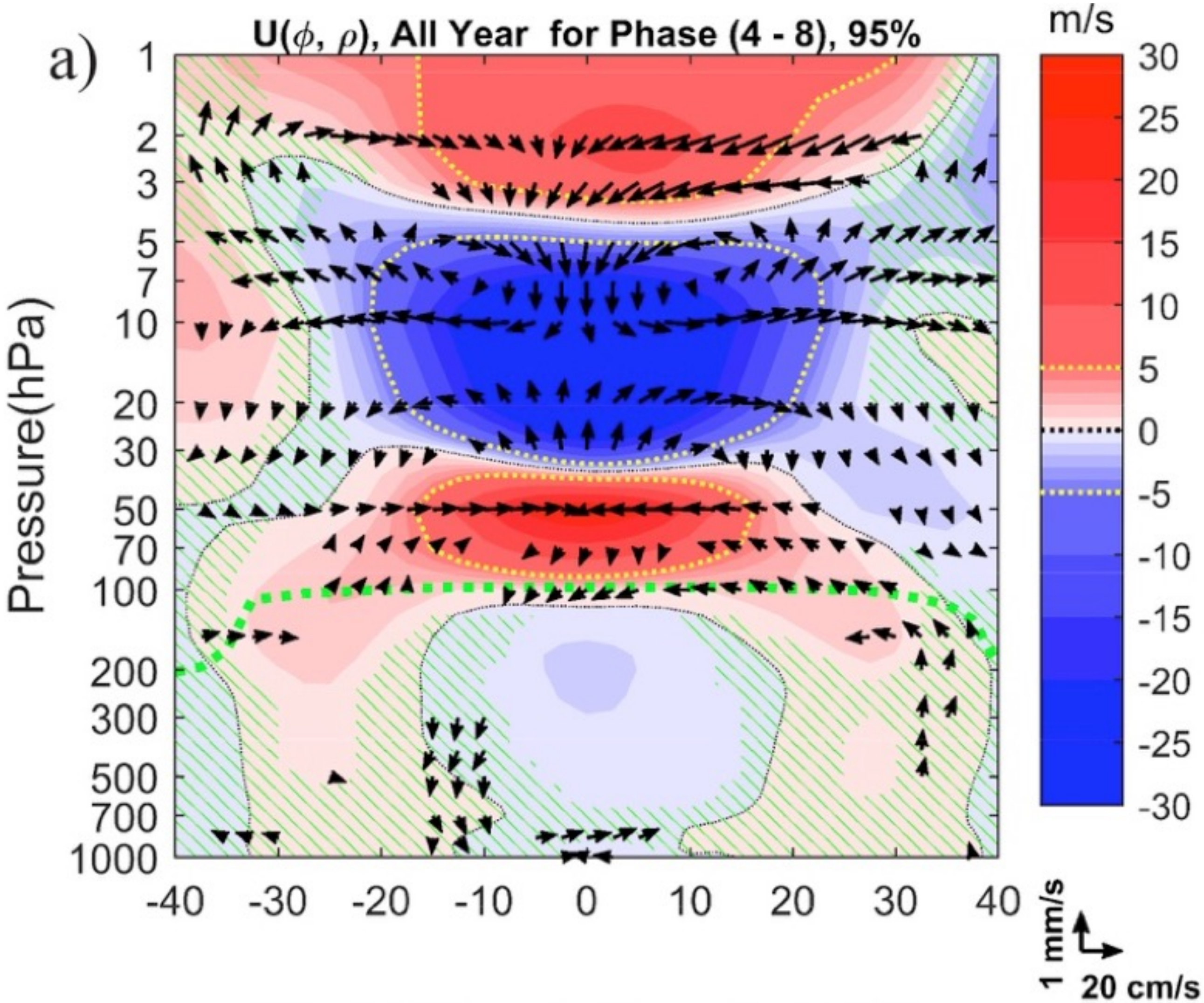

Hitchman, M. H., S. Yoden, P. H. Haynes, V. Kumar, and S. Tegtmeier, 2021: An observational history of the direct influence of the stratospheric Quasi-biennial Oscillation on the tropical and subtropical upper troposphere and lower stratosphere. J. Meteor. Soc. Japan, 99, https://doi.org/10.2151/jmsj.2021-012

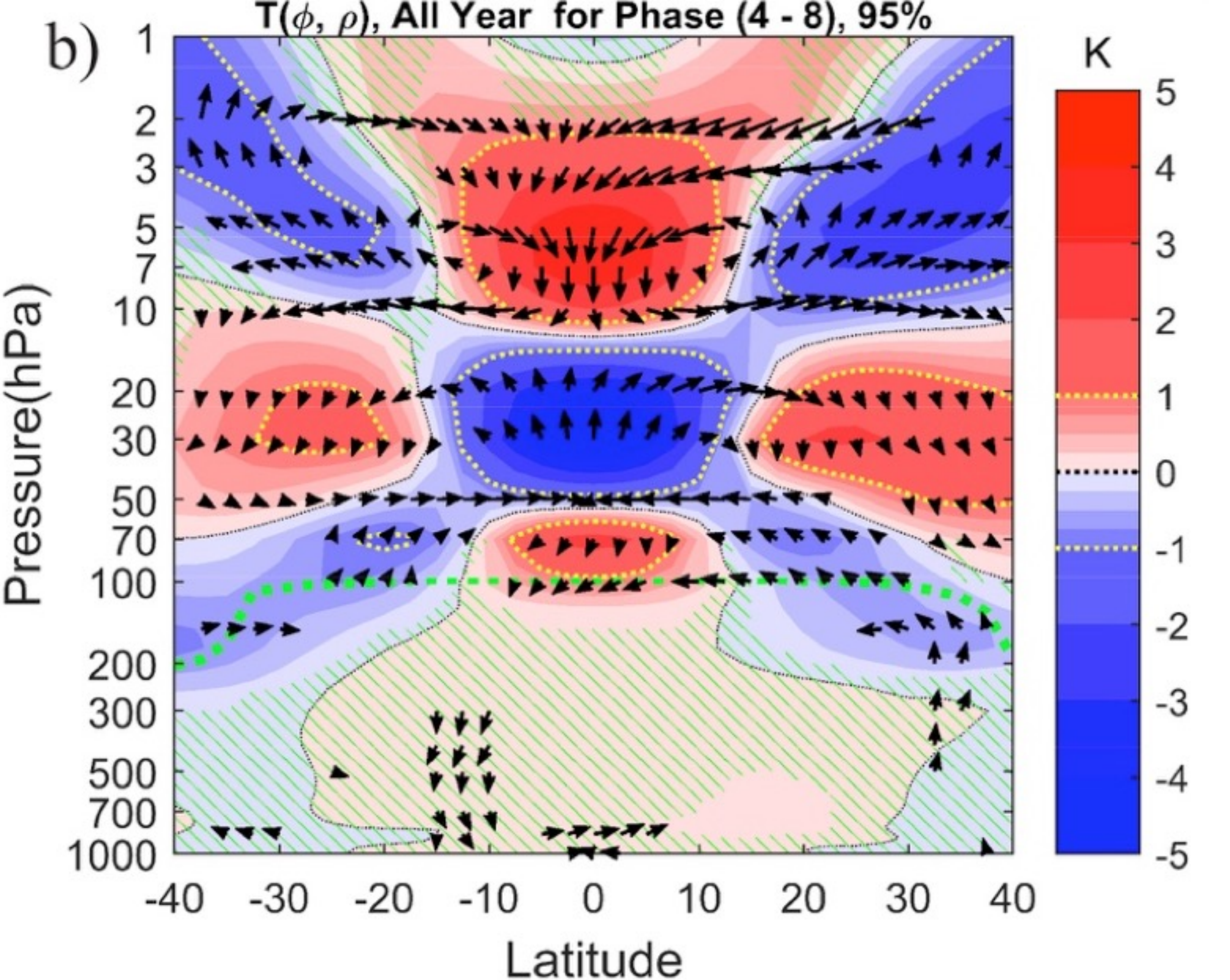

b)
T(ϕ, ρ), All Year for Phase (4 - 8), 95%
Pressure(hPa)
1
2
3
5
7
10
20
30
50
70
100
200
300
500
700
1000
-40
-30
-20
-10
0
10
20
30
40
Latitude
K
5
4
3
2
1
0
-1
-2
-3
-4
-5

How does air exit the tropics?

Middle Stratosphere Fall Winter Spring

Planetary scale waves

Lower Stratosphere All Year

Monsoon tops interact with
travelling baroclinic waves

Regulated by the phase of the QBO

Trepte (1993)

SAGE II Aerosol Extinction Ratio 570 K

~23 km

23 June - 25 July 1991, sunset

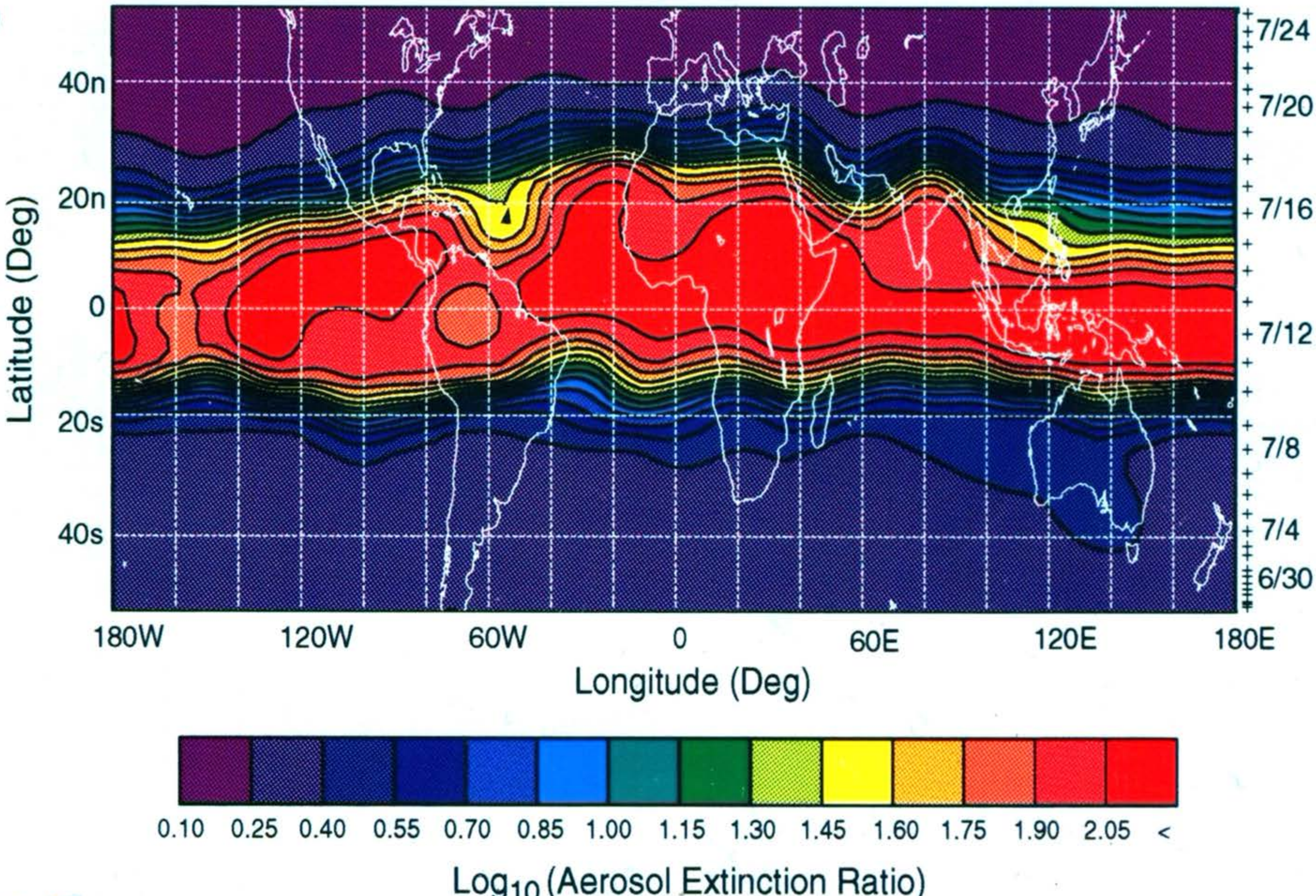

Trepte et al. (1993)   JGR

June 14 – July 26, 1991 SAGE II

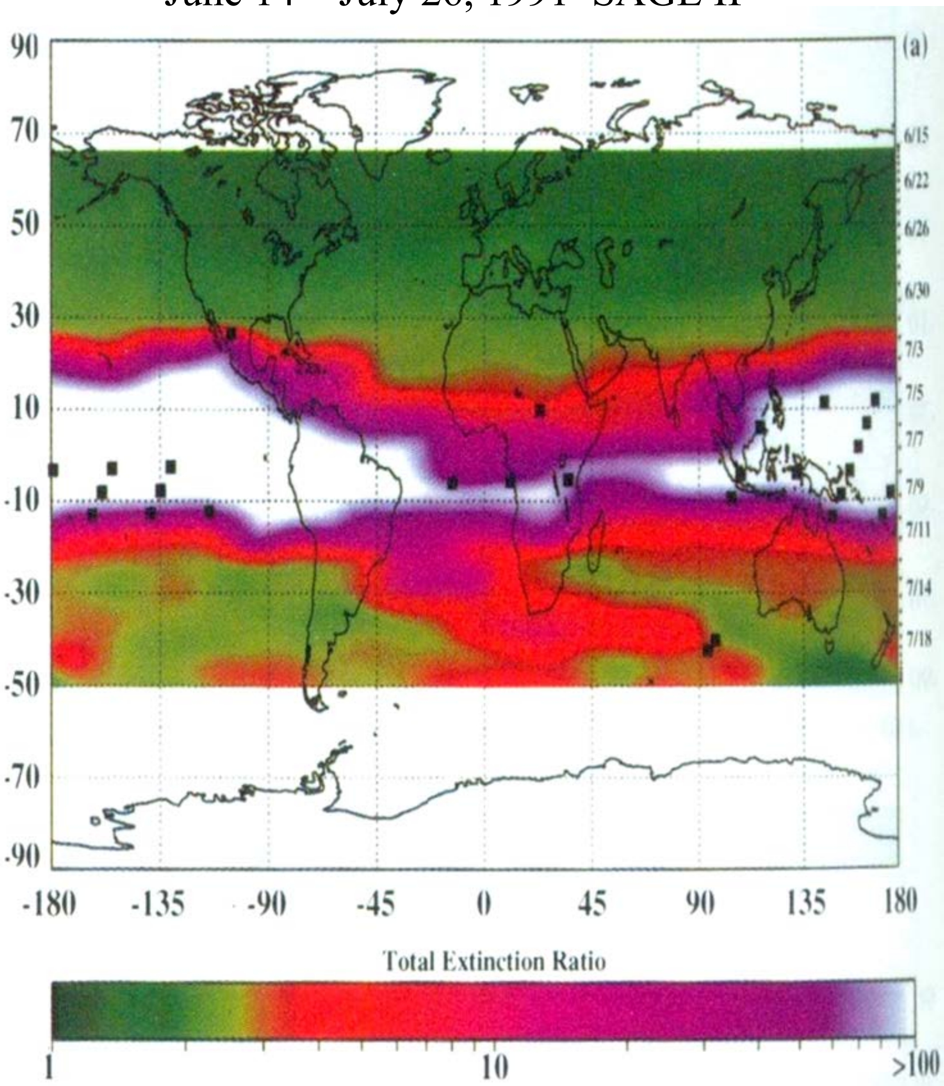

570 K ~ 23 km altitude

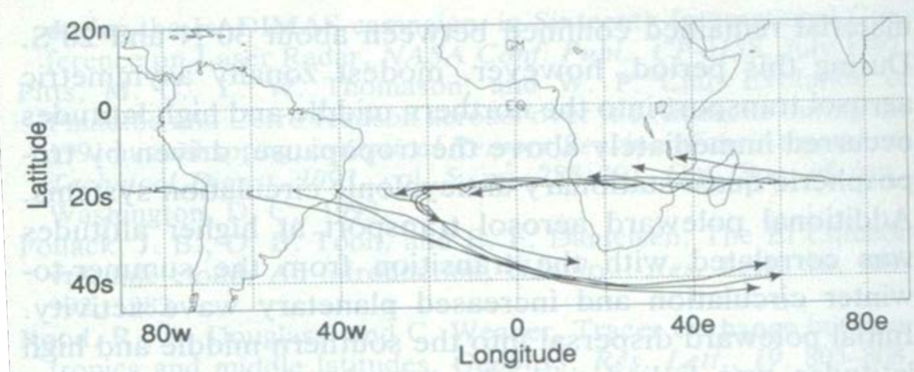

Fig. 7. Isentropic trajectory analysis at 570 K for the period July 10–16, 1991. Parcels were initiated at 20°S and separated by 10° in longitude.

Eruptions change the general circulation of the stratosphere

- Increased Brewer-Dobson Circulation
  → more methane in stratosphere
- Cooler troposphere → drier troposphere
- Warmer tropical tropopause
  → more water vapor in stratosphere
- Warmer tropical stratosphere
- More polar stratospheric clouds
- Warm continental troposphere in winter

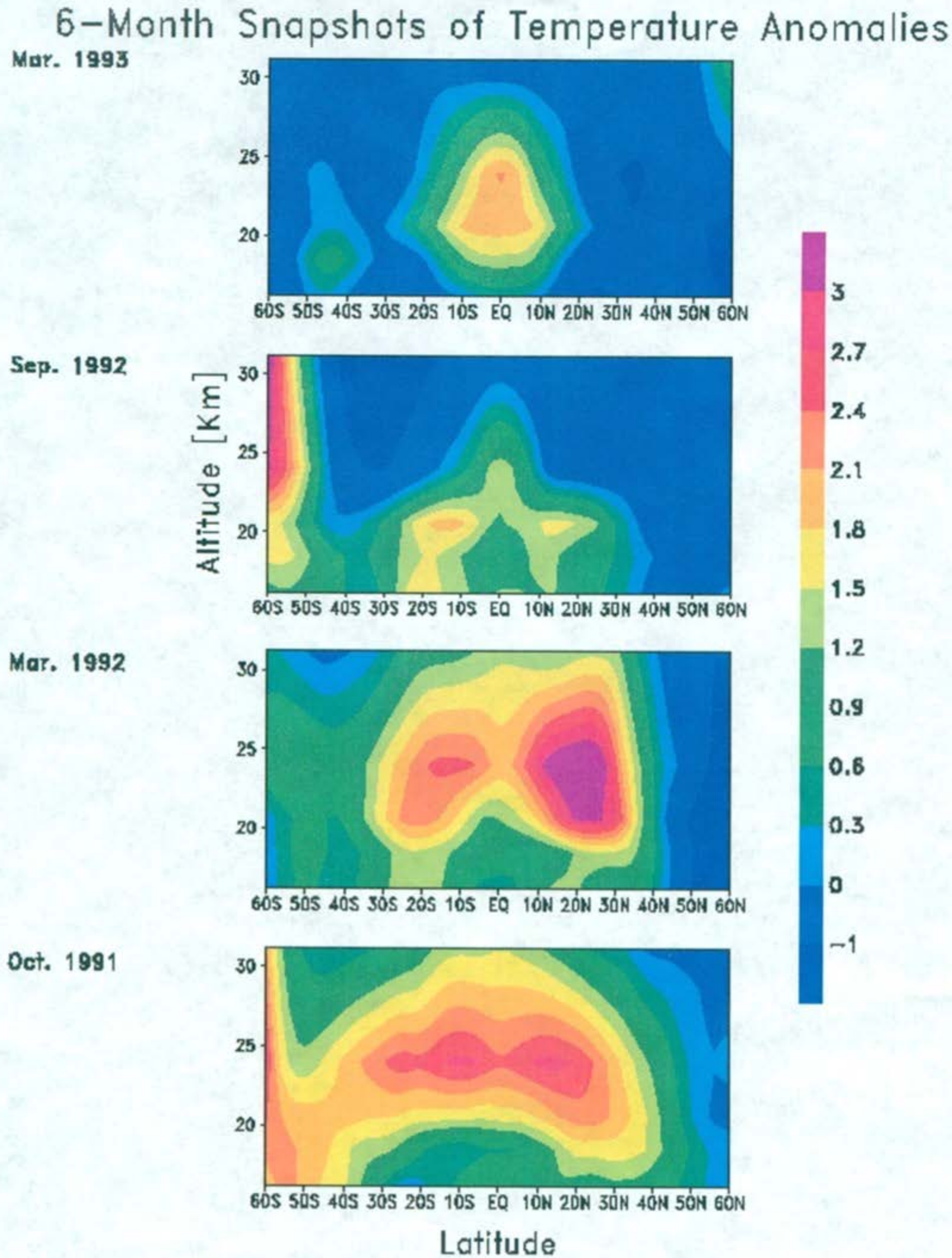

6-Month Snapshots of Temperature Anomalies
Mar. 1993
Sep. 1992
Mar. 1992
Oct. 1991
Altitude [Km]
30
25
20
60S 50S 40S 30S 20S 10S EQ 10N 20N 30N 40N 50N 60N
Latitude
3
2.7
2.4
2.1
1.8
1.5
1.2
0.9
0.6
0.3
0
−1

TABLE 3. Effects of Large Explosive Volcanic Eruptions on Weather and Climate

Effect	Mechanism	Begins	Duration
Reduction of diurnal cycle	blockage of shortwave and emission of longwave radiation	immediately	1–4 days
Reduced tropical precipitation	blockage of shortwave radiation, reduced evaporation	1–3 months	3–6 months
Summer cooling of NH tropics and subtropics	blockage of shortwave radiation	1–3 months	1–2 years
Stratospheric warming	stratospheric absorption of shortwave and longwave radiation	1–3 months	1–2 years
Winter warming of NH continents	stratospheric absorption of shortwave and longwave radiation, dynamics	$\frac{1}{2}$ year	one or two winters
Global cooling	blockage of shortwave radiation	immediately	1–3 years
Global cooling from multiple eruptions	blockage of shortwave radiation	immediately	10–100 years
Ozone depletion, enhanced UV	dilution, heterogeneous chemistry on aerosols	1 day	1–2 years

Robock (2000) Rev. Geophys.

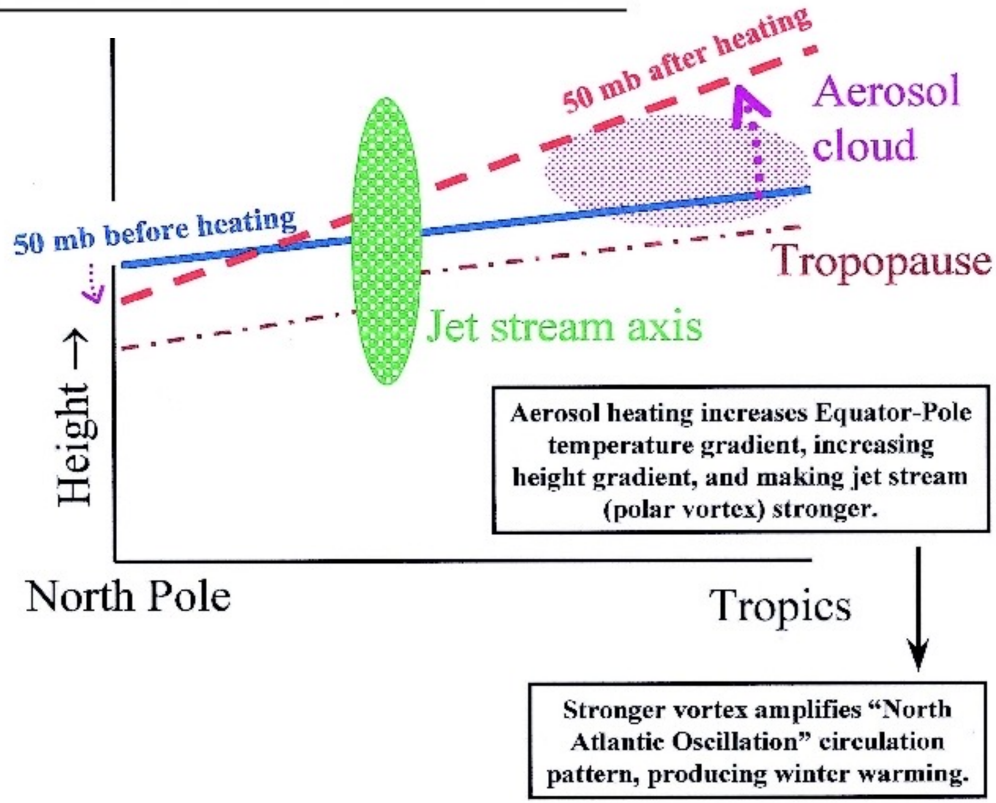

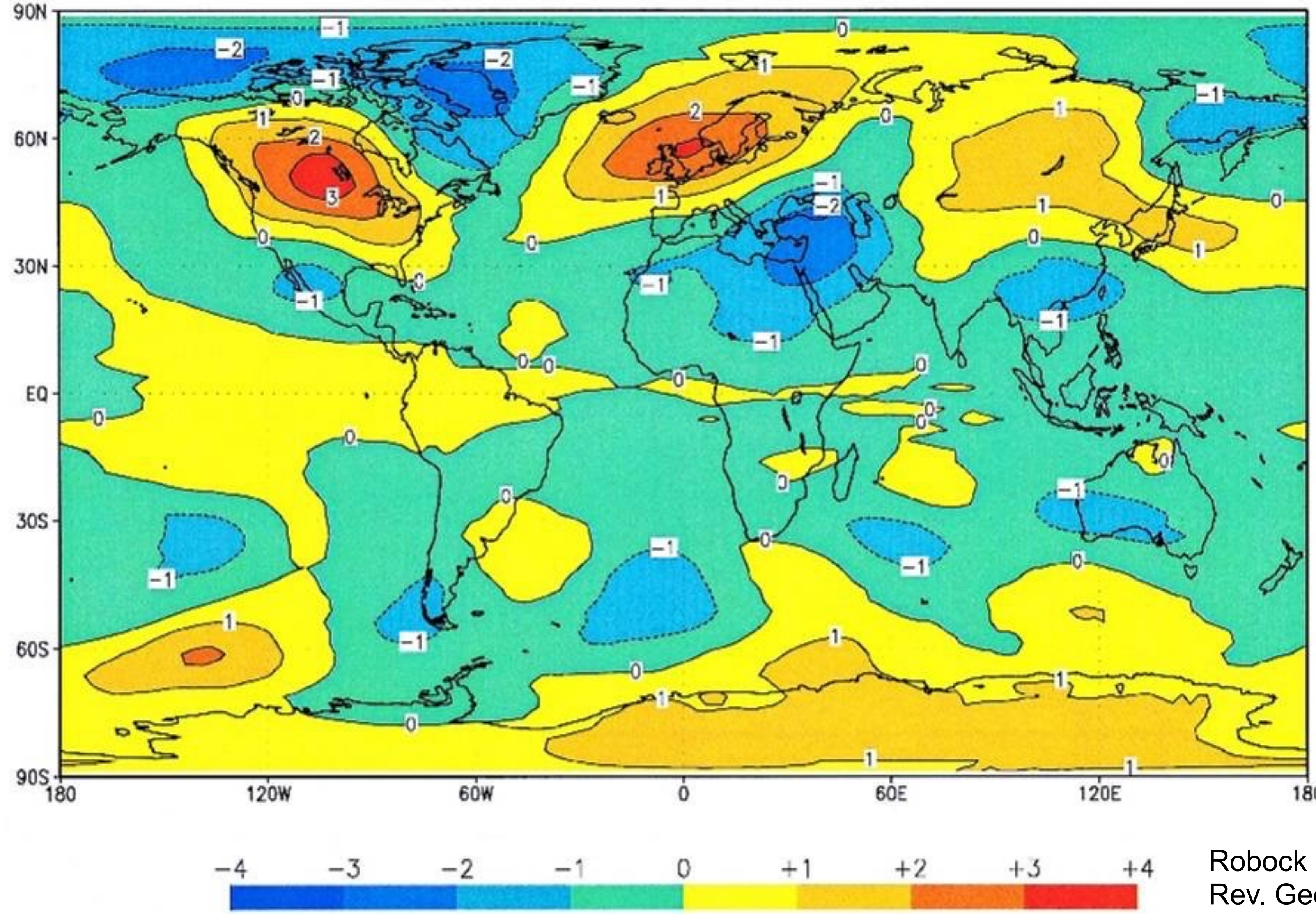

Robock (2000)
Rev. Geophys.

Plate 8. Winter (December-January-February (DJF)) lower tropospheric temperature anomalies (with the nonvolcanic period of 1984–1990 used to calculate the mean) for the 1991–1992 Northern Hemisphere (NH) winter following the 1991 Mount Pinatubo eruption. This pattern is typical of that following all large tropical eruptions, with warming over North America, Europe, and Siberia and cooling over Alaska, Greenland, the Middle East, and China. Data are from microwave sounding unit channel 2R [*Spencer et al.*, 1990], updated courtesy of J. Christy and now called channel 2LT.

Baldwin and Dunkerton (2001)
Science

Northern Annular Mode
(~NAO, AO)

Sea Level Pressure - Mean

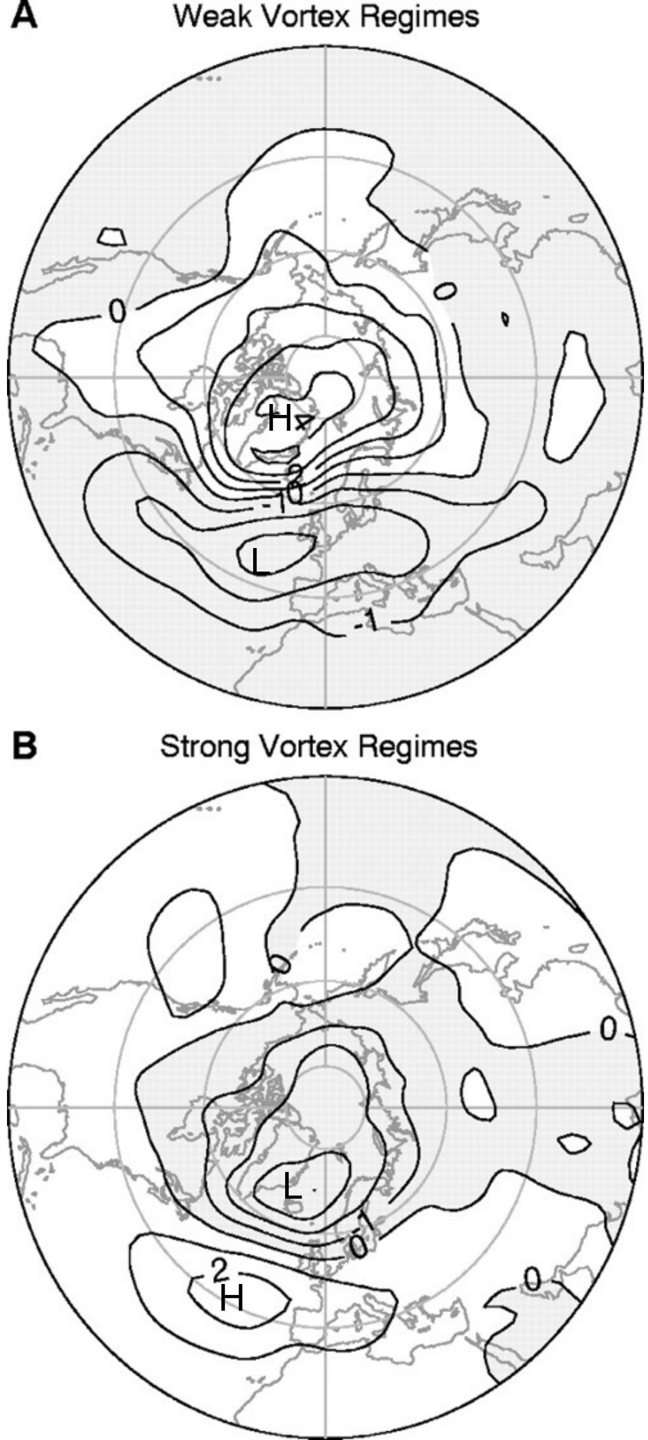

Baldwin and Dunkerton (2001) Science

Blue = Stronger westerly vortex

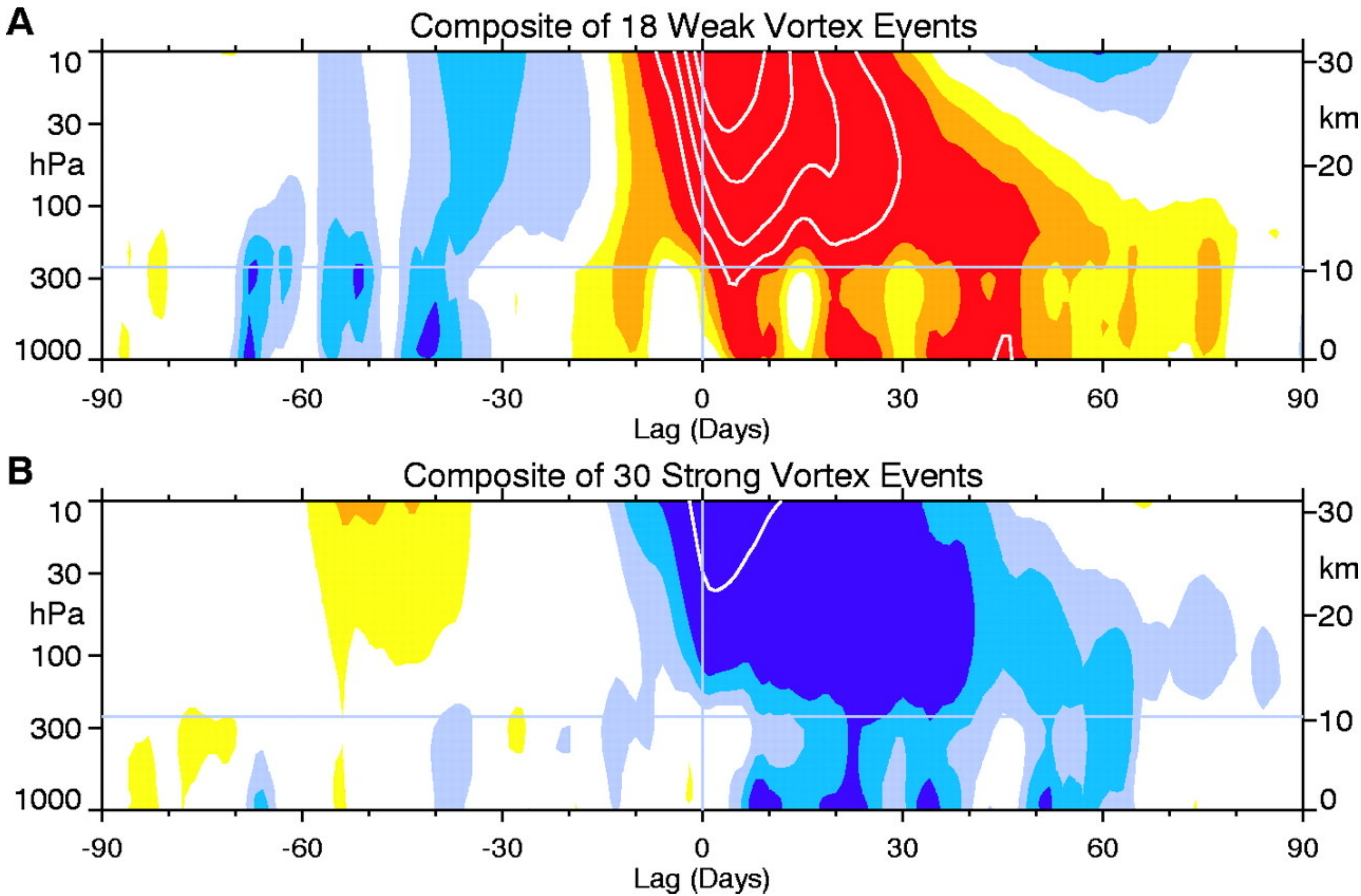

Shindell et al. 2004: Climate response to eruptions since 1600. *J. Geophys. Res.*, **109**.

Table 1. Years of Large Volcanic Eruptions[a]

Year	Name and Latitude	Radiative Forcing	RF3	RF1	RM92
1600	Huaynaputina, 17 S	−5.43	X	X	
1641	Parker, 6 N	−5.50	X	X	
1815	Tambora, 8 S	−5.98	X	X	
1831	Several tropical and midlatitude	−4.86	X	X	
1835	Cosiguina, 13 N	−2.95		X	
1843	Sangay, 2 S, Guntur, 7 S Reventador 0 S	−1.50		X	
1883	Krakatau, 6 S	−3.70	X	X	X
1886	Tarawera, 38 S	0.00			X
1888[b]	Bandai, 38 N	0.00			X
1902	Santa Maria, 15 N	−3.60	X	X	X
1907[b]	Ksudach, 52 N	−0.37			X
1912[b]	Katmai, 58 N	−2.08			X
1932[b]	Quizapu, 36 S	0.00			X
1956[b]	Bezymianny, 56 N	−0.41			X
1963	Agung, 8 S	−0.64/−1.19		X	X
1974	Fuego, 14 N	−0.90			X
1982	El Chichón, 17 N	−2.41/−3.06	X	X	X
1991	Pinatubo, 15 N	−1.60/−3.73	X	X	X
	Average forcing		−4.48	−3.77	−1.59

[a]Radiative forcing comes from the data set of *Crowley* [2000], based on ice cores prior to 1960 and on optical measurements thereafter. While that record showed a large forcing in 1601 (the value given in the table), we believe this must have been the well-known eruption of Huaynaputina in 1600 and have used the surface temperatures in that year instead. Note that during the optically derived period (post-1960), the data set has larger forcing values for major eruptions during the year after the eruption (the second value shown). This is not the case for the ice core derived portion of the record, and we believe this results from the differing time-resolving capabilities of the two methods.

[b]For comparison with *Robock and Mao* [1992], surface temperatures during the second winter following this midlatitude or high-latitude eruption were used. Note that there were two additional lesser eruptions in the Caribbean in 1902.

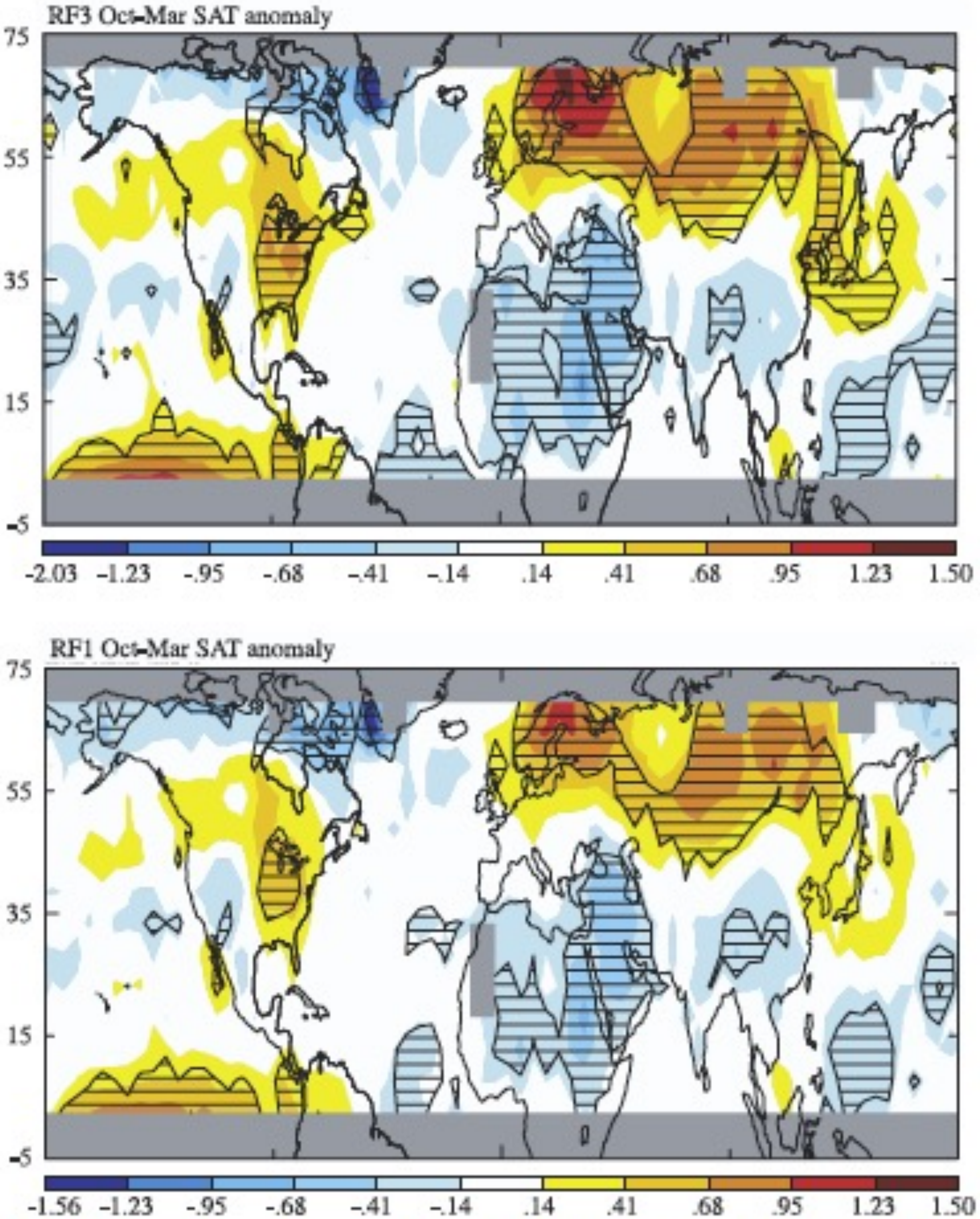

Figure 2. Mean surface temperature anomalies (C) during the cold season (October–March) following large tropical volcanic eruptions averaged over many eruptions. Anomalies are averaged over years with known tropical eruptions with a negative radiative forcing of at least 3 W/m^2 (top) or at least 1 W/m^2 (bottom) relative to the background. See Table 1 for years included in each analysis. Hatched regions indicate areas where the response is significant at the 95% confidence level. Data sources as in Figure 1. Grey areas indicate regions where data were not available.

- Volcanic aerosol patterns reveal the QBO and annual circulations
- Detrainment from the "tropical reservoir" in the mid-stratosphere occurs during winter in association with planetary waves
- Detrainment occurs in the lower stratosphere all year in association with monsoons and travelling synoptic waves
- Major eruption increase the Brewer-Dobson circulation and excite the NAM

Very Large Eruptions

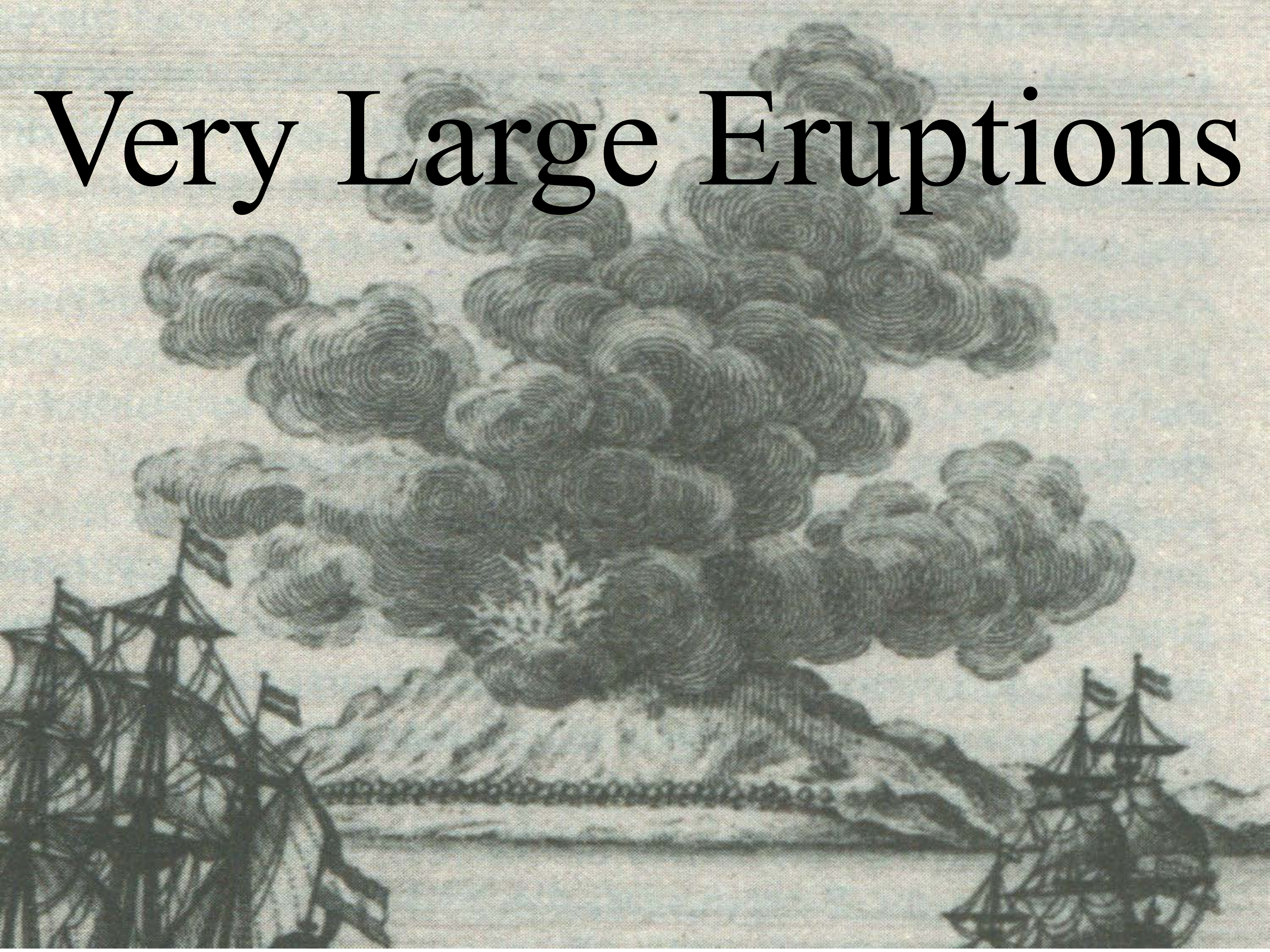

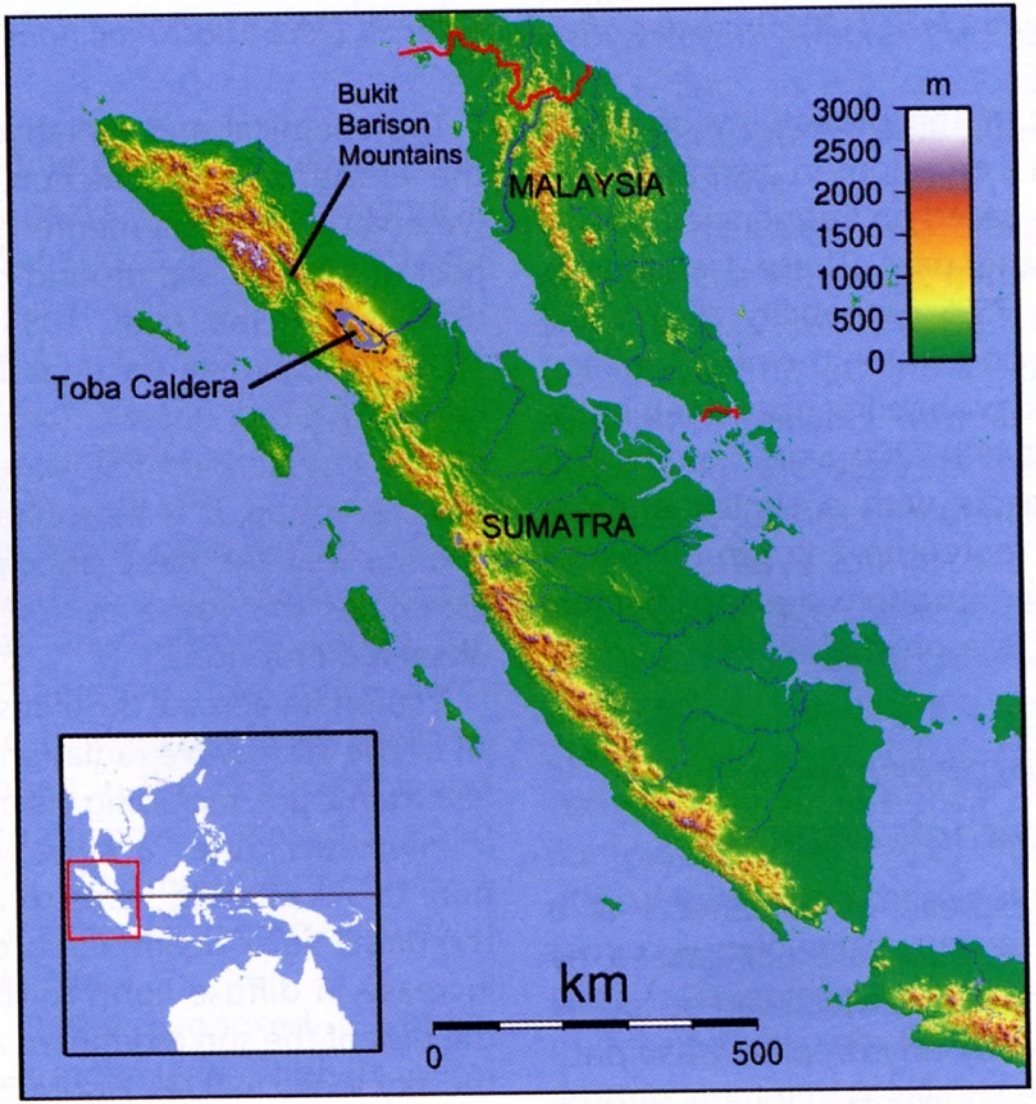

Figure 1. Map of Sumatra showing the location of the Toba Caldera. The caldera itself is 100 km × 40 km and is mostly filled by Lake Toba. Samosir Island, which lies in the centre of the lake, is the result of subsequent uplift following the Younger Toba Tuff eruption around 74 kya. (Base map produced by 'Sadelmelik' and licensed under the Creative Commons Attribution ShareAlike license versions 3.0, 2.5, 2.0, and 1.0. For original image see http://en.wikipedia.org/wiki/Image:Sumatra Topography.png).

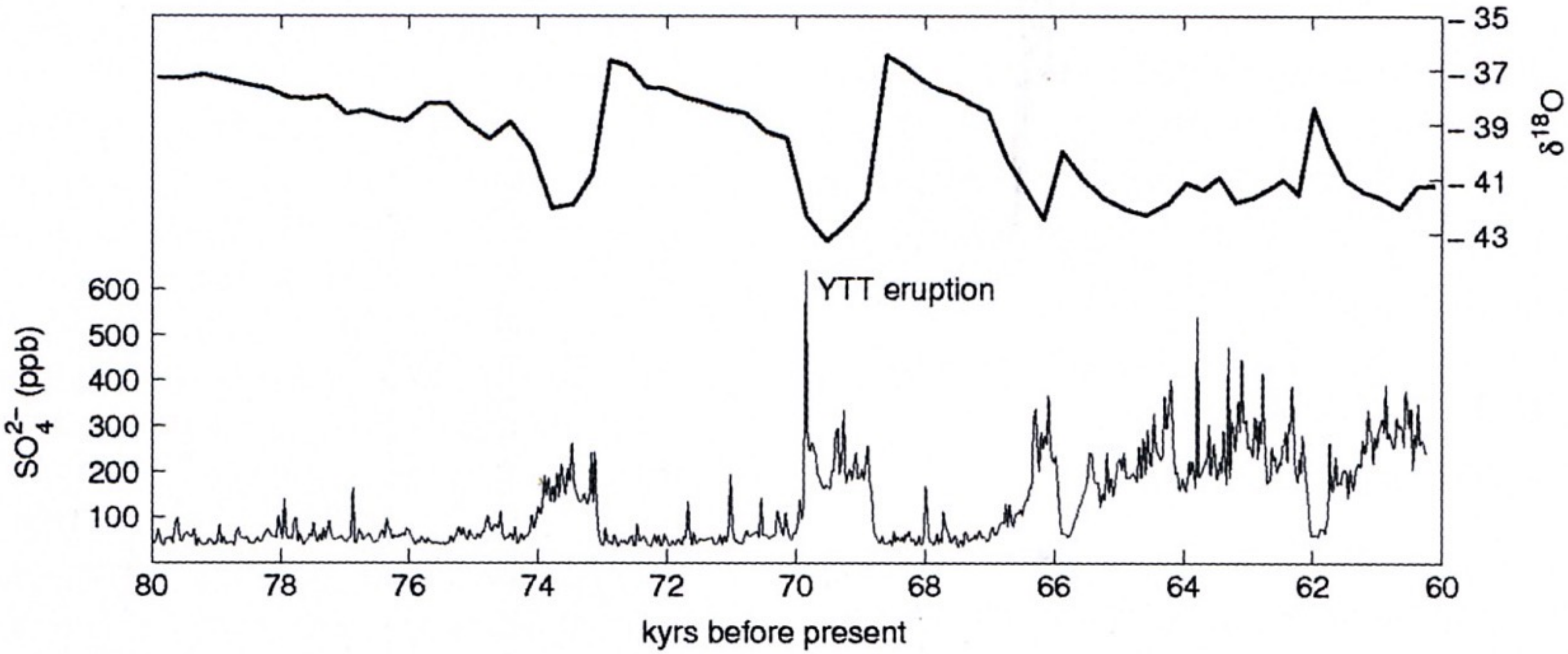

Figure 5. Oxygen isotope data and sulphate measurements from the GISP2 ice core between 60 and 80 kyr ago. The bottom sulphate core shows a clear spike at around 70 kyr ago which is associated with the YTT eruptions. This sulphate spike coincides with a dip in the oxygen isotope ratios, indicating a cooling at that time. The ice core is measured in layers and the isotope ratio is given at the age of the midpoint of each layer. This period covers a transition from warm climate to an ice age with two inter-stadial events. (Figure is based on Figure 4 of Oppenheimer (2002); data from Grootes and Stuiver (1997); Grootes et al.,*(1993); Mayewski et al., (1990, 1997); provided by the National Snow and Ice Data Center, University of Colorado at Boulder, and the World Data Center-A for Paleoclimatology, National Geophysical Data Center, Boulder, Colorado.)*

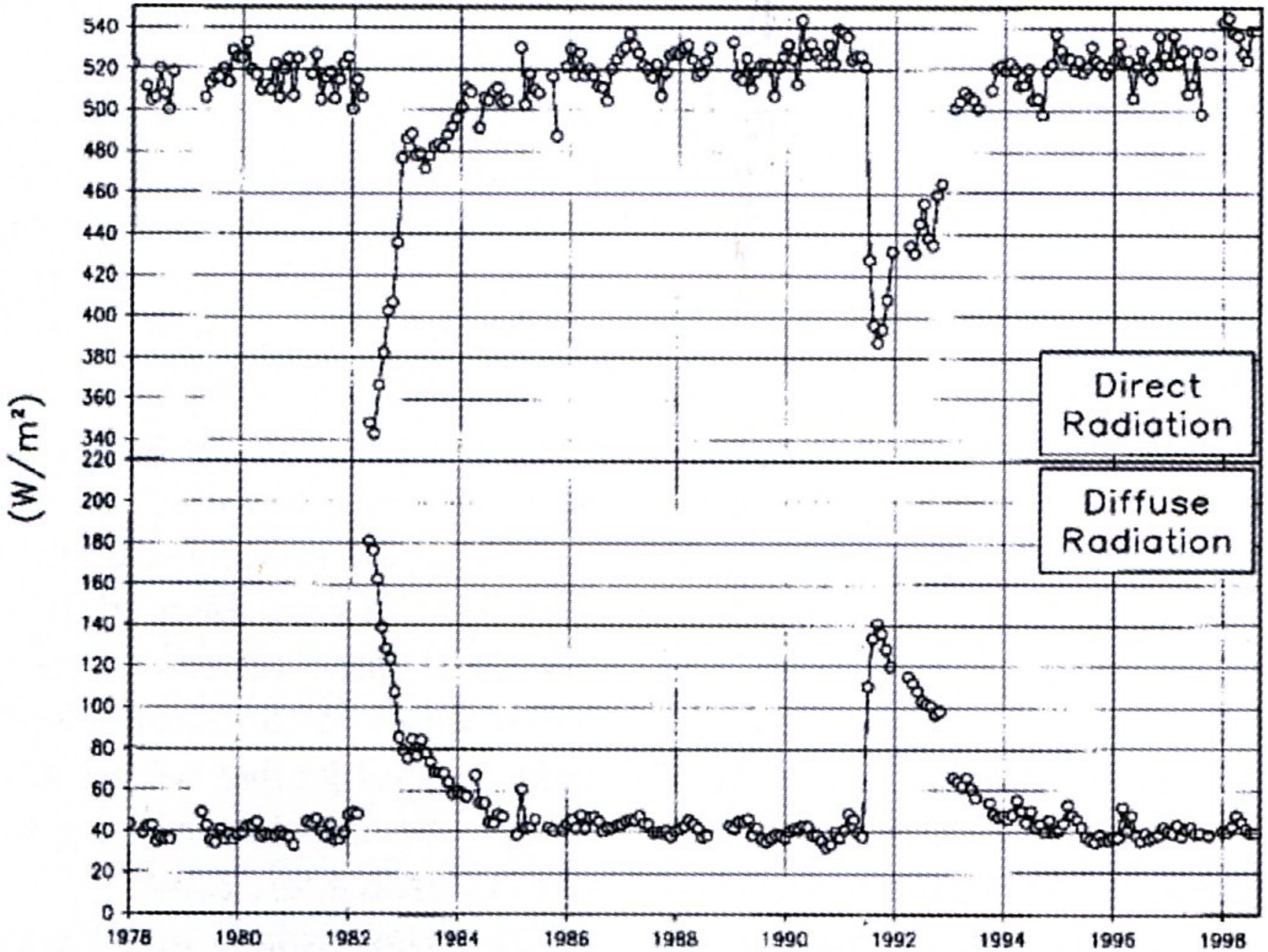

Figure 3. Direct and diffuse broadband radiation measured at the Mauna Loa observatory in Hawaii by a tracking pyroheliometer and a shade disk pyranometer at a solar zenith angle of 60° during clear-sky conditions. The spikes in 1982 and 1991 show changes in radiation following the eruptions of El Chichon and Pinatubo. The years on the abscissa represent January of that year. (Figure taken from Figure 2 in Robock (2000).)

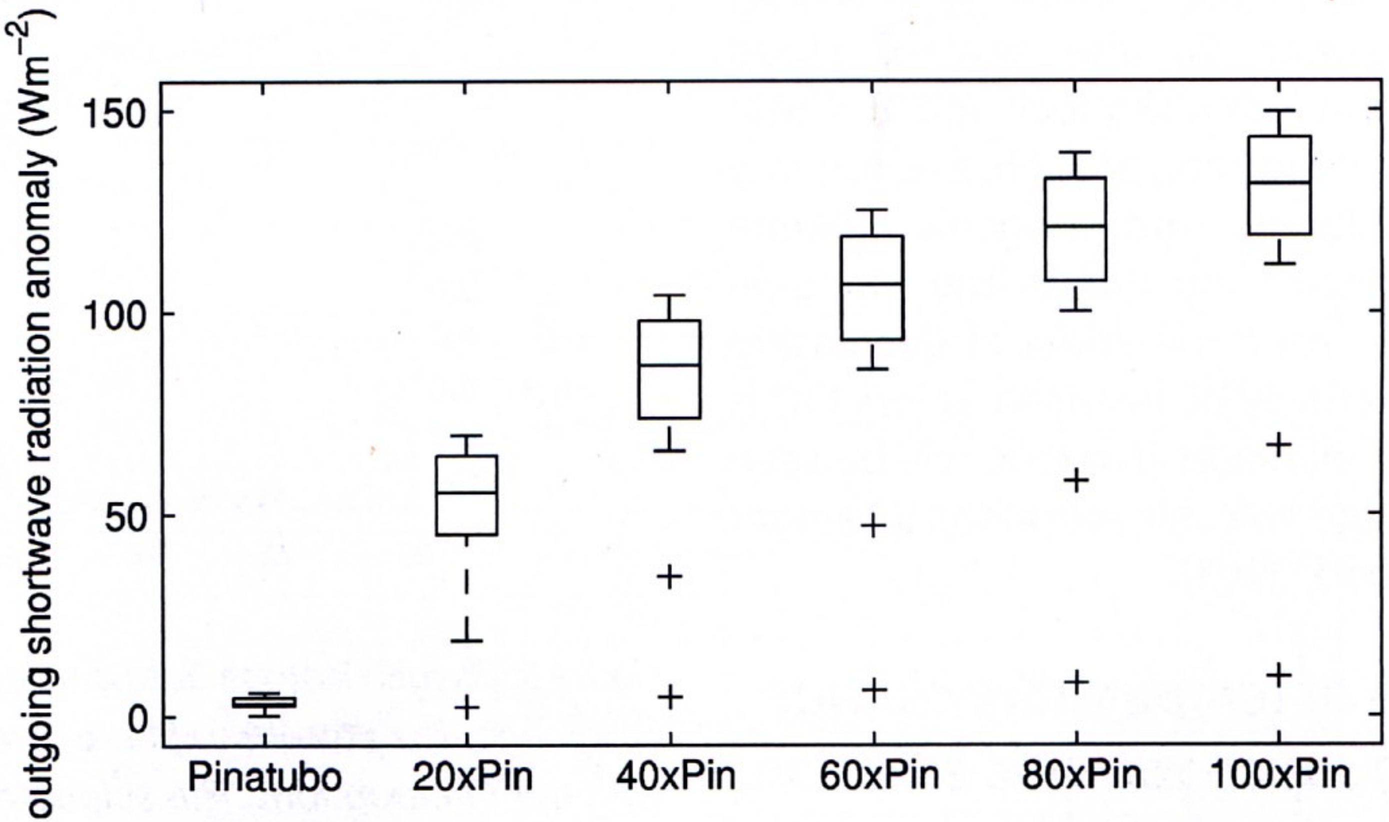

Figure 7. Outgoing shortwave radiation anomaly at the top of the atmosphere following six different volcanic eruptions simulated in the Met Office Unified Model with a slab ocean (HadSM3). Each box represents the greatest proportion of global monthly mean values (upper quartile to lower quartile) for the two years following each eruption; whiskers indicate the minimum and maximum values and outliers are represented by crosses. The relative increase in outgoing shortwave radiation in each case is not directly proportional to the mass of sulphate aerosol from that eruption.

Slab ocean

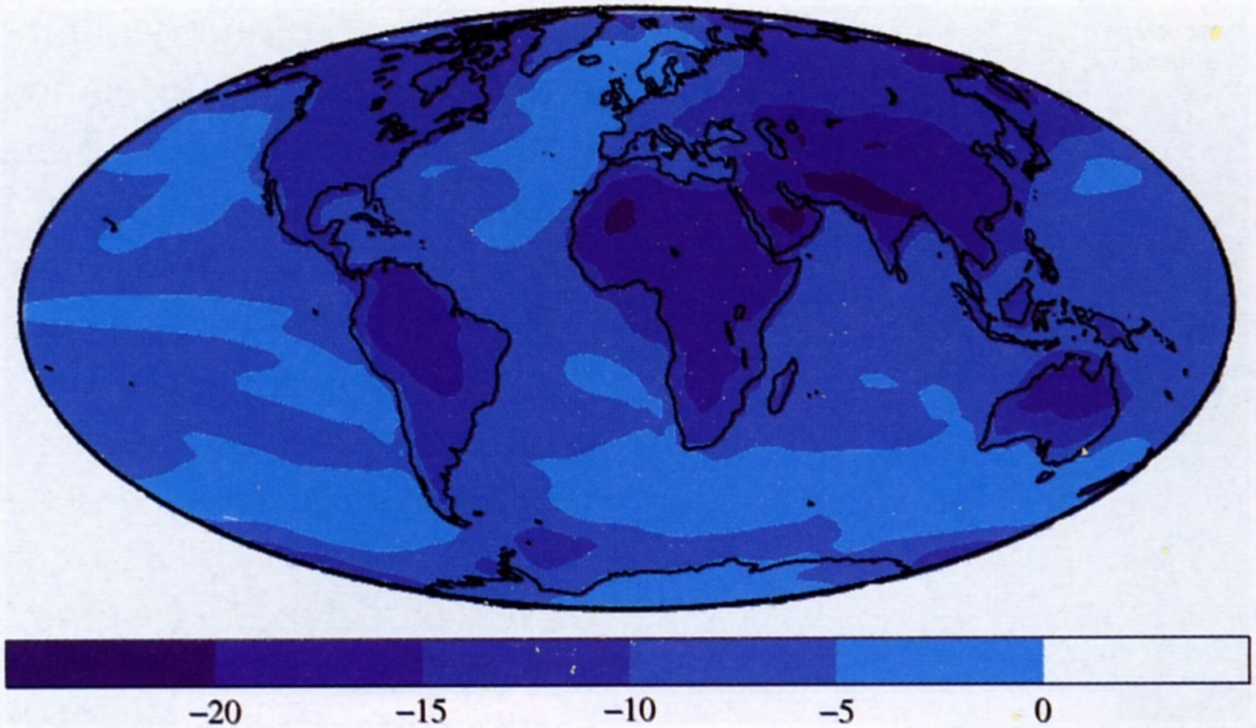

Figure 6. Surface temperature anomalies a year following a super-eruption simulated in a global circulation (climate) model study conducted by Jones et al., (2005). Cooling over land is greater than cooling over ocean and reaches over 20 degC over Africa, Saudi Arabia and the Himalayas. Most land areas are cooled by at least 10 degC. (© Figure supplied by and reproduced with permission from Gareth Jones, UK Met Office Hadley Centre.)

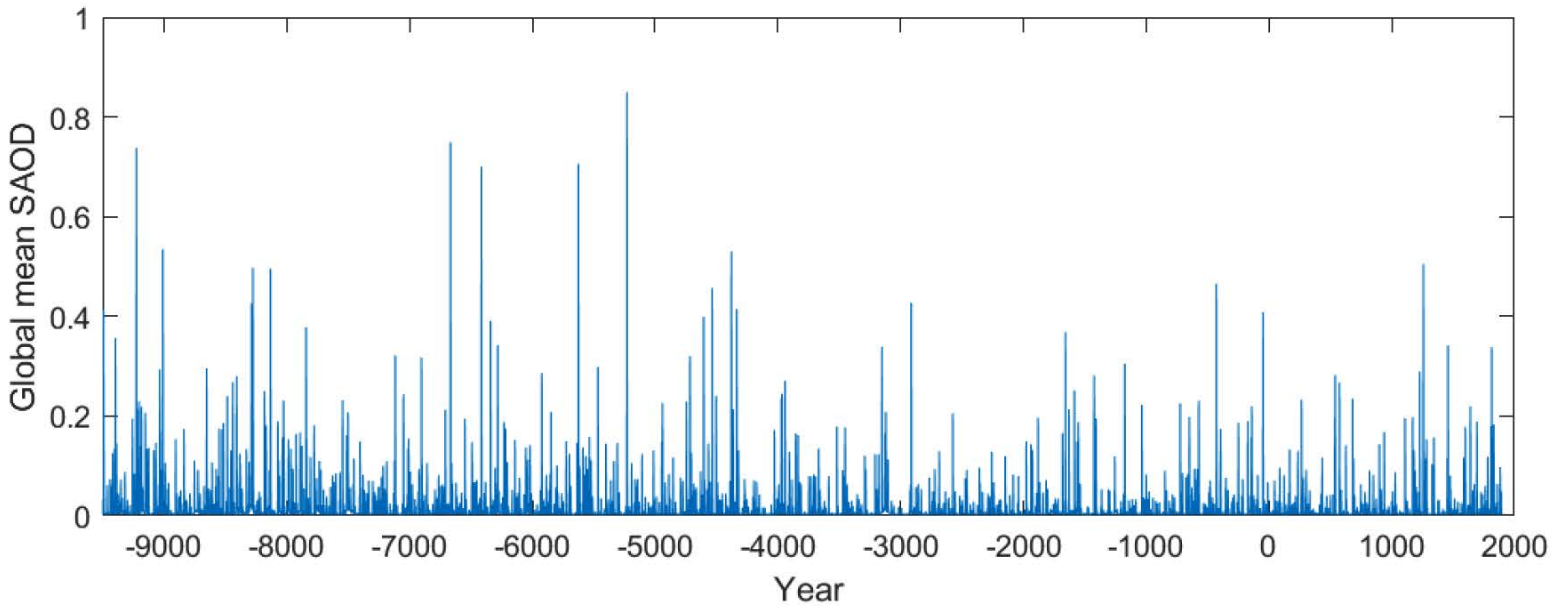

Figure 9: Global mean annual mean stratospheric aerosol optical depth (SAOD) from the EVA(HolVol) reconstruction. Years are shown using the ISO 8601 standard, which includes a year zero.

Sigl, et al. 2022, Earth System Science Data

2 ice cores; $-0.25\ to\ -1\ W/m^2$

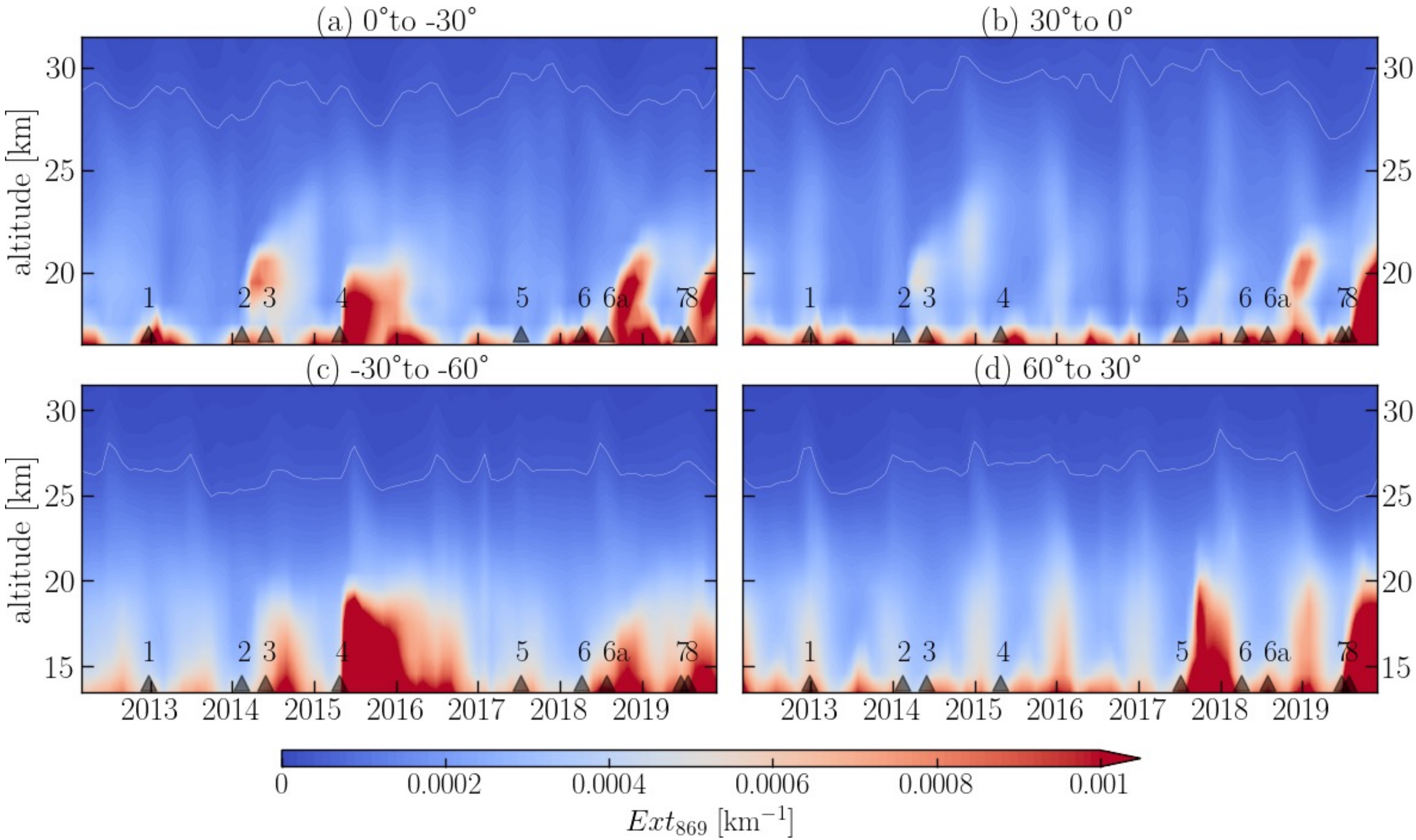

Malinina et al., 2021, ACP

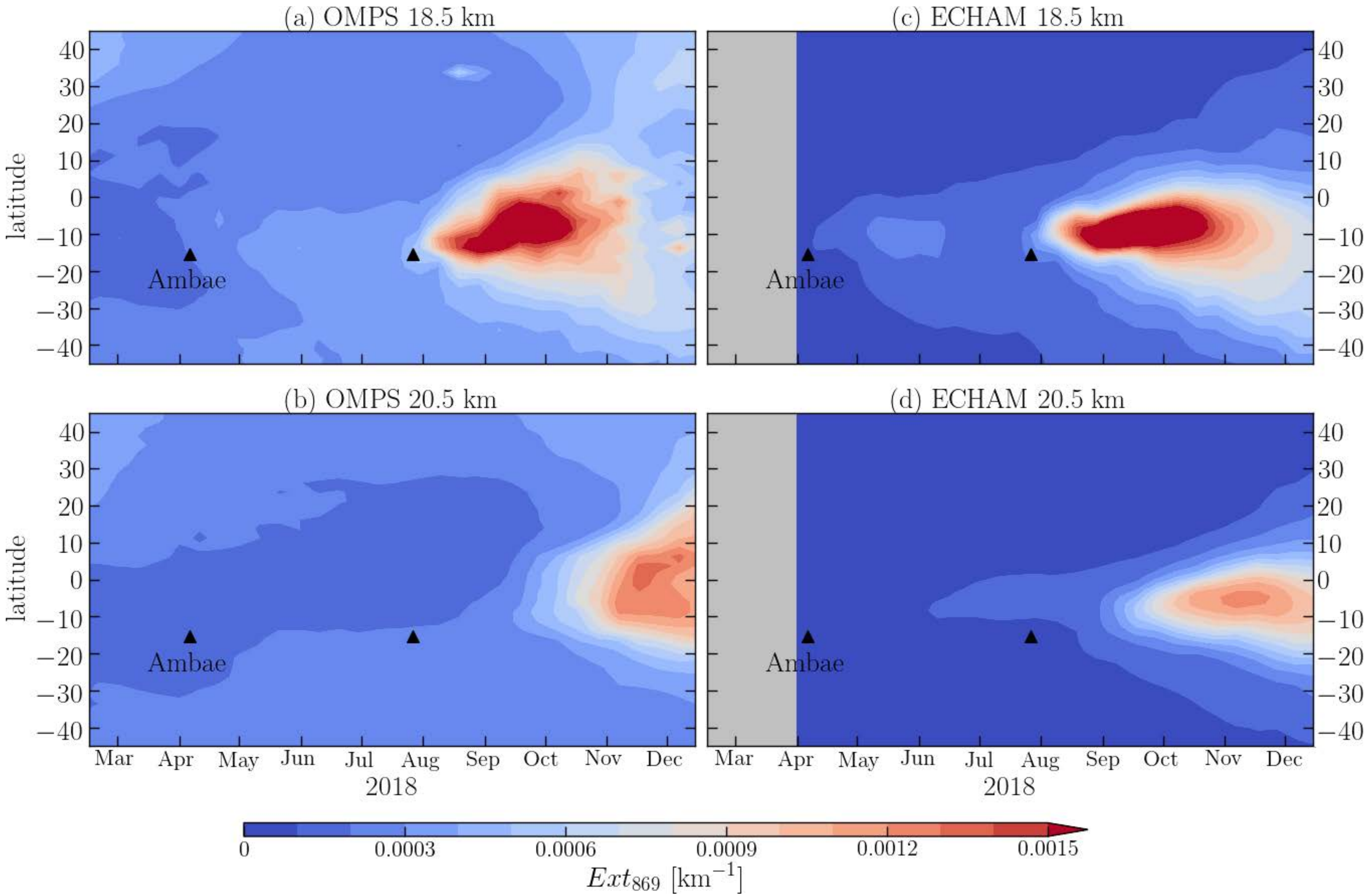

Changes in stratospheric aerosol extinction coefficient after the 2018 Ambae eruption as seen by OMPS-LP and MAECHAM5-HAM

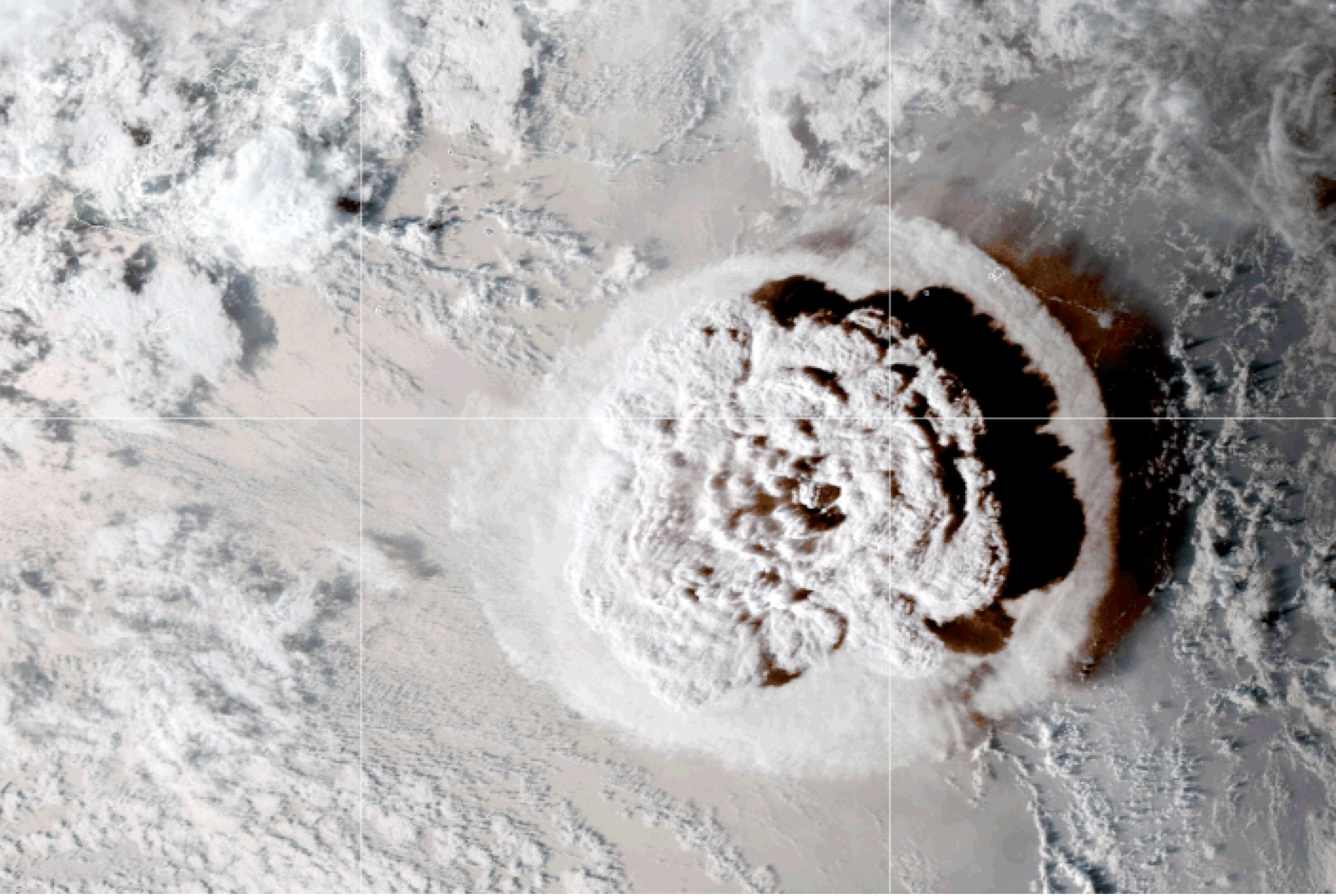

Hunga Tonga-Hunga Ha‘apai January 19, 2022

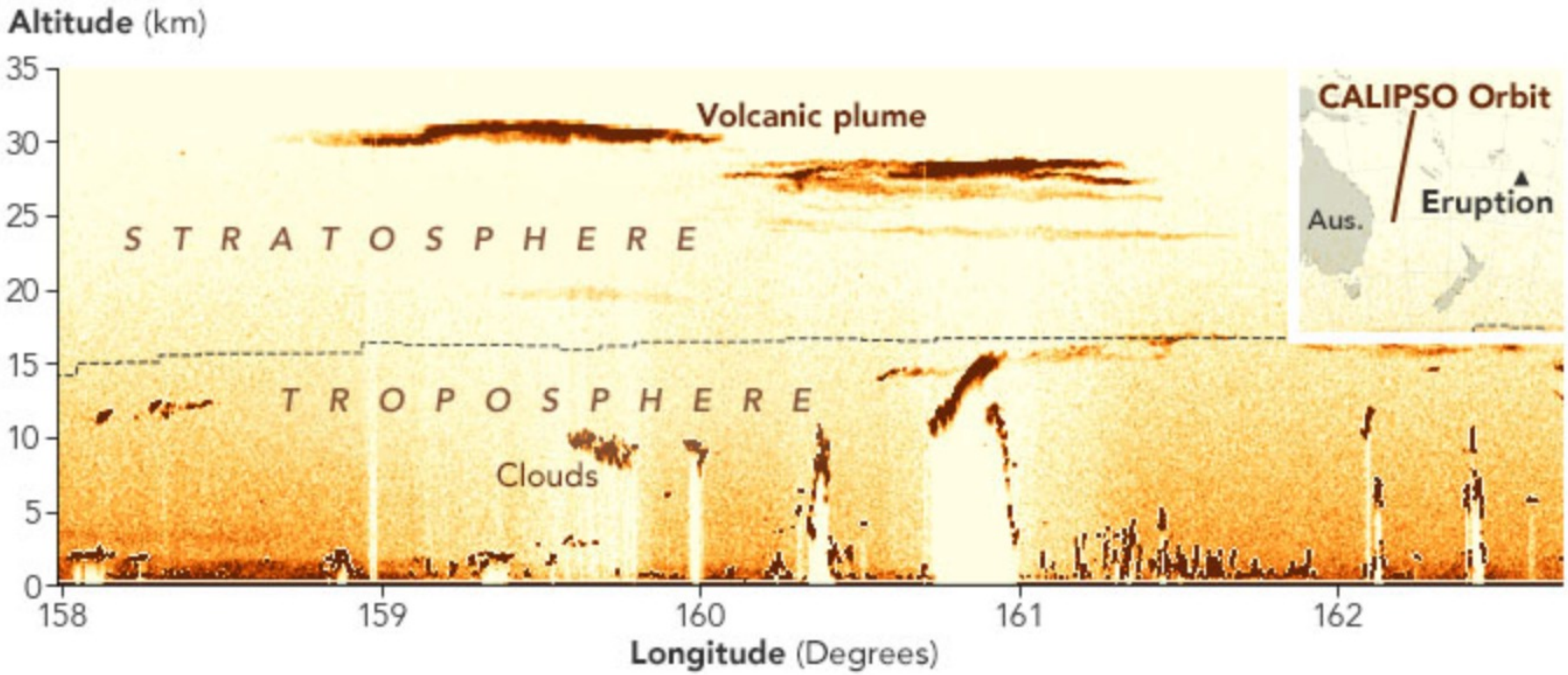

January 16, 2022

The second image, based on data collected on January 16 by the Cloud-Aerosol Lidar and Infrared Pathfinder Satellite Observations (CALIPSO) mission, shows material from the eruption rising to an altitude of 31 kilometers (19 miles). Other CALIPSO data collected on January 15 indicates that a small amount of ash and gas may have reached as high as 39.7 kilometers (24.7 miles).